CHEMISTRY
A EUROPEAN JOURNAL

DOI: 10.1002/chem.200902552

Chelation versus Binucleation: Metal Complex Formation with the Hexadentate *all-cis*-N^1,N^2-Bis(2,4,6-trihydroxy-3,5-diaminocyclohexyl)ethane-1,2-diamine

Mark Bartholomä, Sergej Gisbrecht, Stefan Stucky, Christian Neis, Bernd Morgenstern, and Kaspar Hegetschweiler*[a]

Dedicated to Professor Hans-Jörg Schneider on the occasion of his 75th birthday

Abstract: The hexadentate ligand *all-cis*-N^1,N^2-bis(2,4,6-trihydroxy-3,5-diaminocyclohexyl)ethane-1,2-diamine (L^e) was synthesized in five steps with an overall yield of 39% by using $[Ni(taci)_2]SO_4\cdot 4H_2O$ as starting material (taci = 1,3,5-triamino-1,3,5-trideoxy-*cis*-inositol). Crystal structures of $[Na_{0.5}(H_6L^e)](BiCl_6)_2Cl_{0.5}\cdot 4H_2O$ (**1**), $[Ni(L^e)]Cl_2\cdot 5H_2O$ (**2**), $[Cu(L^e)](ClO_4)_2\cdot H_2O$ (**3**), $[Zn(L^e)]CO_3\cdot 7H_2O$ (**4**), $[Co(L^e)](ClO_4)_3$ (**5c**), and $[Ga(H_{-2}L^e)]NO_3\cdot 2H_2O$ (**6**) are reported. The Na complex **1** exhibited a chain structure with the Na^+ cations bonded to three hydroxy groups of one taci subunit of the fully protonated $H_6(L^e)^{6+}$ ligand. In **2**, **3**, **4**, and **5c**, a mononuclear hexaamine coordination was found. In the Ga complex **6**, a mononuclear hexadentate coordination was also observed, but the metal binding occurred through four amino groups and two alkoxo groups of the doubly deprotonated $H_{-2}(L^e)^{2-}$. The steric strain within the molecular framework of various $M(L^e)$ isomers was analyzed by means of molecular mechanics calculations. The formation of complexes of L^e with Mn^{II}, Cu^{II}, Zn^{II}, and Cd^{II} was investigated in aqueous solution by using potentiometric and spectrophotometric titration experiments. Extended equilibrium systems comprising a large number of species were observed, such as $[M(L^e)]^{2+}$, protonated complexes $[MH_z(L^e)]^{2+z}$ and oligonuclear aggregates. The pK_a values of $H_6(L^e)^{6+}$ (25 °C, $\mu = 0.10$ M) were found to be 2.99, 5.63, 6.72, 7.38, 8.37, and 9.07, and the determined formation constants ($\log\beta$) of $[M(L^e)]^{2+}$ were 6.13(3) (Mn^{II}), 20.11(2) (Cu^{II}), 13.60(2) (Zn^{II}), and 10.43(2) (Cd^{II}). The redox potentials (vs. NHE) of the $[M(L^e)]^{3+/2+}$ couples were elucidated for Co (−0.38 V) and Ni (+0.90 V) by cyclic voltammetry.

Keywords: amino alcohols · bridging ligands · chelates · coordination modes · N,O ligands

Introduction

Triamine ligands with a cyclic backbone that are restricted to facial coordination have received much interest, owing to possible applications in catalysis and in particular as mimetics for the modeling of the active site of metalloproteins.[1–3] The connection of two trinuclear units via a polymethylene $(CH_2)_n$ ($n \geq 2$) linker generates a potentially hexadentate chelator that could either form mononuclear hexacoordinated or dinuclear bis-triscoordinated species. For the tridentate 1,4,7-triazacyclononane and its methylated derivative, a variety of such coupled chelators has been described in the literature, and a series of mono- and polynuclear metal complexes of several transition metal cations have been characterized.[4] To the best of our knowledge, this approach has not widely been exploited for other cyclic triamine ligands.[5] The linking of two *all-cis*-1,3,5-triaminocyclohexane (tach) units by an ethylene bridge has been the main focus of a PhD work.[6] However, the results have not been published in a scientific journal. More recently, the preparation and metal binding properties of two dimeric derivatives of the related 1,3,5-triamino-1,3,5-trideoxy-*cis*-inositol (taci) have been reported.[7] In these compounds, rigid and separating linker units that prevent coordination of six donor atoms to one metal cation were used.

[a] Dr. M. Bartholomä, Dipl.-Chem. S. Gisbrecht, Dr. S. Stucky, Dr. C. Neis, Dr. B. Morgenstern, Prof. Dr. K. Hegetschweiler
Anorganische Chemie, Universität des Saarlandes
Postfach 15 11 50, 66041 Saarbrücken (Germany)
Fax: (+49) 681-302-2663
E-mail: hegetschweiler@mx.uni-saarland.de

Supporting information for this article is available on the WWW under http://dx.doi.org/10.1002/chem.200902552.

Taci is a versatile ligand because of the high number of functional groups, leading to an N,N,N (i), N,O,N (ii), O,N,O (iii), or O,O,O (iv) coordination mode (Scheme 1a). In addition, the oxygen donors can bind a metal ion either as neutral hydroxy groups or in the form of a zwitter ion, as alkoxo groups (proton transfer from a coordinated oxygen donor to a non-coordinated nitrogen donor, see Scheme 1b).[8] We expected a corresponding dimer bearing a suitable linker to be a particularly interesting metal complexing agent. In view of the different possible interactions of a metal ion with hydroxy and amino groups, it would be intriguing to elucidate whether a mononuclear chelation or a polynuclear aggregation takes place for a particular metal cation. Co^{III} complexes with a bis-taci-ligand have been prepared recently in our laboratory by a template method.[9] However, in these complexes, the two taci subunits were interlinked by N=CH−NH−CH_2−NH or NH−CH_2−C(NH_2)=N bridges, which are sensitive to hydrolysis as soon as the metal center is removed. Herein, we report on the synthesis of a stable ethylene-bridged bis-taci derivative L^e, and on its complex formation with Na^I, Ni^{II}, Cu^{II}, Zn^{II}, Co^{III}, and Ga^{III} in the solid state and in solution.

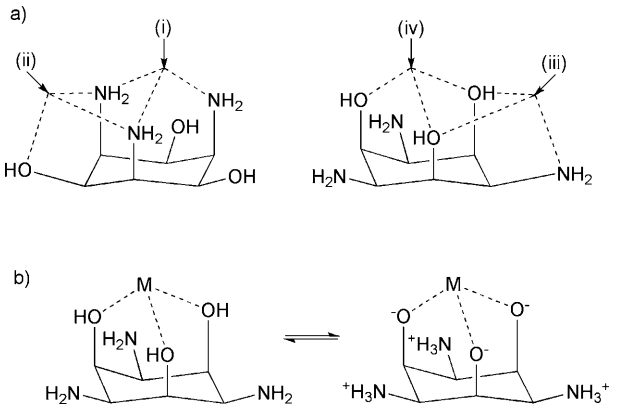

Scheme 1. Possible coordination modes of 1,3,5-triamino-1,3,5-trideoxy-*cis*-inositol.

Results and Discussion

Preparation and characterization of the ligand: In view of the high number of potentially nucleophilic donor groups, selective alkylation of taci is not trivial. We have previously described the preparation of the urea derivative **P3** (Scheme 2) of taci, which has only one free amino group.[10] This derivative proved to be particularly suitable for the coupling reaction required for the tethering of two taci units. Since sufficient solubility of **P3** is only achieved in water and methanol, a reductive amination reaction with glyoxal and sodium borohydride, which can be performed in water, was used. The yield of this reaction was only moderate (68%); however, the unreacted monomer **P3** can be readily separated from the dimer **P4** and can be re-used for the synthetic procedure without significant loss. The final removal of the protecting urea group requires harsh conditions, such as reflux in an ethylene glycol/water mixture at high NaOH concentration and high temperature. The bis-taci ligand L^e was isolated as a hydrated hydrochloride $L^e{\cdot}6HCl{\cdot}2.5H_2O$ and was fully characterized by elemental analysis and spectroscopic methods. The ^1H and ^{13}C NMR spectra of $H_x(L^e)^{x+}$ ($0 \le x \le 6$) all contain five resonances (Figure 1), which is in agreement with symmetry considerations.[11] Assignments were established by a series of ^1H–^1H and ^1H–^{13}C correlation experiments. The vicinal J_{C-H} coupling interactions H1/C5 and H5/C1 that were observed in the ^1H–^{13}C long-range spectrum are an unambiguous proof that the linking of the two taci fragments has indeed been achieved.

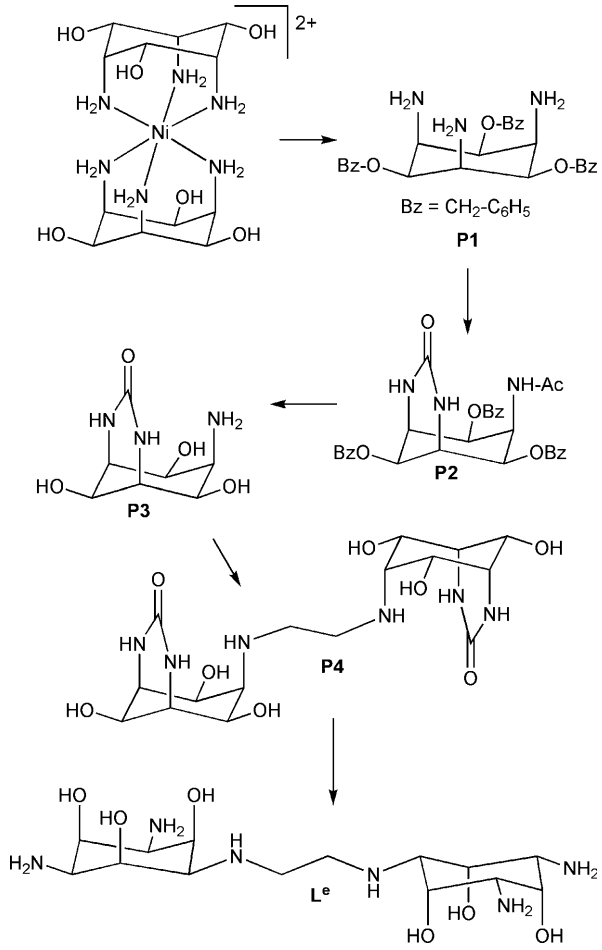

Scheme 2. Synthetic pathway for L^e.

The fully protonated $H_6(L^e)^{6+}$ reacts as a hexaprotic acid, and the corresponding pK_a values have been determined by potentiometric measurements (25 °C) in 0.1 M KCl, 1.0 M KCl and 1.0 M KNO_3 (Table 1). It is known that highly protonated polyaza macrocycles can bind anions in solution.[12] However, the pK_a values of $H_6(L^e)^{6+}$ do not vary significantly for the 1.0 M KCl and 1.0 M KNO_3 medium, indicating that $H_6(L^e)^{6+}$···anion interactions are mostly negligible. The marked dependence of the pK_a values on the inert electrolyte concentration is in accordance with the well-known de-

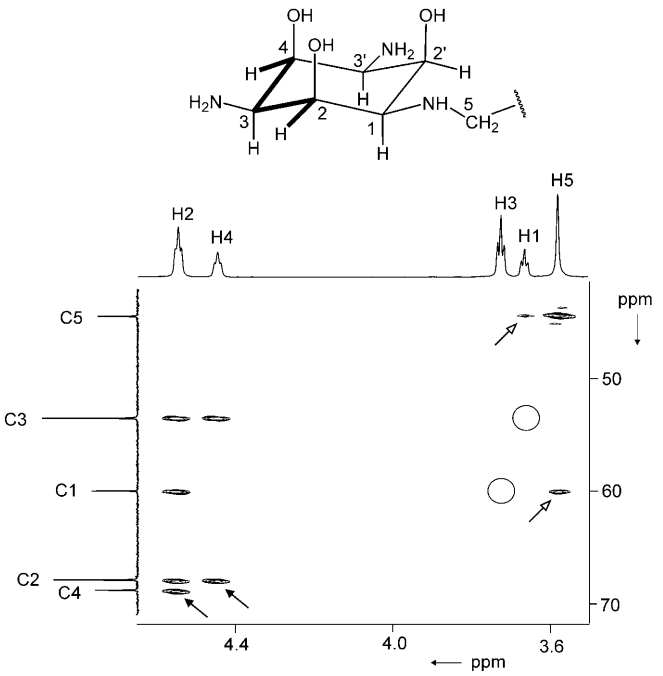

Figure 1. Long range C–H correlated 2D NMR spectrum of $H_x(L^e)^{x+}$ ($x \approx 5.6$) at pH* = 3.0.[43] The significant H2–C4 and H4–C2 coupling (black arrows) and the non-observance of H1–C3 and H3–C1 coupling (circles) indicate a chair conformation with axial hydroxy groups; the H1–C5 and H5–C1 couplings (white arrows) prove the interlinking of the two taci moieties by an ethylene bridge. The numbering scheme is given in the structural representation on top. In this representation the observed long-range C–H interactions indicative of the chair conformation with axial hydroxy groups are highlighted as bold bonds.

Table 1. Equilibrium constants for the stepwise protonation of L^e (log K_i)[a,b] at 25 °C in aqueous media. Values for L^{mx}, L^{px} and taci (25 °C) are shown for comparison.

	L^{e}[c]			L^{mx}[d]	L^{px}[d]	taci[e]
	0.1 M KCl	1.0 M KCl	1.0 M KNO_3	0.1 M NaCl	0.1 M NaCl	0.1 M KCl
$\log K_6$	2.99	3.46	3.53	4.99	5.26	
$\log K_5$	5.63	6.10	6.14	5.67	5.65	
$\log K_4$	6.72	7.15	7.15	6.73	6.95	
$\log K_3$	7.38	7.71	7.75	7.33	7.65	5.96
$\log K_2$	8.37	8.63	8.63	8.39	8.87	7.42
$\log K_1$	9.07	9.17	9.22	8.98	9.30	8.91

[a] $K_i = [LH_i] \times [H]^{-1} \times [LH_{i-1}]^{-1}$. [b] For the sake of comparability, the values are given here as protonation constants K_i; the usual pK_a values are obtained by $pK_{ai} = \log K_{n+1-i}$ with $n = 6$ for L^e, L^{mx}, L^{px} and $n = 3$ for taci. [c] This work, estimated standard deviations are 0.01 or less. [d] Reference [7]. [e] Reference [31].

0.1 M KCl) was performed (Figure 2). However, line broadening or splitting of individual resonances have not been observed. Moreover, significant coupling for C4/H2 and C2/H4 on one hand and non-observance of such coupling interactions between C3/H1 and C1/H3 on the other hand (Figure 1) were found for the entire pH range investigated. All these observations indicate a single conformation for the two cyclohexane rings with axial oxygen atoms and equatorial nitrogen atoms for the fully and partially protonated and completely deprotonated species. A similar behavior has already been found for the $H_x taci^{x+}$ ($0 \le x \le 3$) monomer.[13] This assignment is further supported by the observed monotonic decrease of the chemical shifts with increasing pH values. It is well established that protonation of a basic site causes a deshielding of the neighboring C–H protons, and this effect increases with a decreasing number of bonds between the basic site and the hydrogen atom under consideration.[14–16] The particularly strong shift observed for H1 and H5 in the range of $2 \le pH \le 4$ together with the negligi-

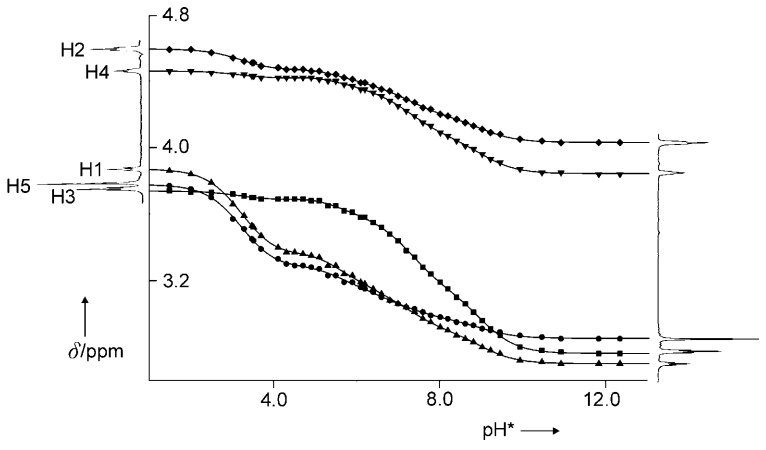

Figure 2. pH* dependence[43] of the ^1H NMR resonances of $H_x(L^e)^{x+}$ ($0 \le x \le 6$). The points correspond to experimental values; the lines were calculated (minimization of $\Sigma[\delta_{obs} - \delta_{calcd}]^2$). The numbering scheme of Figure 1 is used.

pendence of activity coefficients on the ionic strength. The fully protonated $H_6(L^e)^{6+}$ dimer is a considerably stronger acid than the H_3taci^{3+} monomer and the dimeric derivatives $H_6(L^{mx})^{6+}$ and $H_6(L^{px})^{6+}$ (L^{mx}: 1,3-bis(3,5-diamino-cyclohexyl-2,4,6-triol-amino-methyl)benzene, L^{px}: 1,4-bis(3,5-diamino-cyclohexyl-2,4,6-triol-amino-methyl)benzene) reported by Mancin et al.,[7] for which the two taci units are bridged by a *meta*- or *para*-xylene linker unit (Table 1). The low pK_{a1} of $H_6(L^e)^{6+}$ can obviously be explained by the increased electrostatic repulsions, due to the relatively short ethylene tether unit. Moreover, the small ΔpK_a values for the pK_{ai} values with $i \ge 2$ indicate an alternating deprotonation of the two taci subunits in the dimeric system. To further corroborate the deprotonation process and to elucidate possible conformational changes upon deprotonation, an NMR titration experiment in D_2O (25 °C,

ble effect observed for H3 in this range, corroborates the hypothesis of a first selective deprotonation step at the diamino-ethane bridge.

Structure of the metal complexes—molecular mechanics calculations: A large number of structures arise from the different possibilities to wrap the bis-taci molecule around a metal cation. The different stereoisomers of a mononuclear, hexacoordinated chelate $[M(L^e)]^{z+}$ can be classified in terms of the coordination modes adopted by the two taci subunits (Scheme 1). In addition, *cis*/*trans* or *mer*/*fac* diastereomers must be considered for some of these combinations. Further structural diversity arises from the inequivalence of the alkylated and non-alkylated nitrogen donors and the possibility to adopt an *R* or *S* configuration at the coordinated secondary-nitrogen donors. It is obvious that the ethylene bridge is too short to span a *trans*-N-M-N arrangement. Consequently, the corresponding structures, such as a *trans*-bis-type(iii) isomer, were not further considered. For similar reasons, the linking of two non-coordinated nitrogen donors, as required for a bis-type(iv) structure, for example, was also neglected. After exclusion of such highly strained structures, 15 possible isomers **M1**–**M15** were identified (see Table S1 in the Supporting Information). For some of them, different conformations were accounted for, owing to a distinct folding of the chelate rings. Finally, different tautomers were taken into account, owing to the possibility of adopting zwitterionic forms. It is far from trivial to judge the stability of all these species in terms of their free energy of formation ΔG. This quantity would depend on solvation effects, the intrinsic affinity of the selected metal ion for either nitrogen or oxygen donors, and on the steric strain within the coordination sphere and the ligand back bone. As a first screening, we analyzed the steric contributions by means of molecular mechanics calculations and chose Co^{III} as a representative of relatively small metal cations with defined octahedral coordination geometry. It is clear that large metal cations, such as the trivalent lanthanides, could give significantly different results. These calculations revealed a total of six low-energy structures (Scheme 3), with the *trans*-bis-type(ii) structure **M6** being the least strained. The additional low-strain isomers have a bis-type(i), type(i)-type(ii), type(i)-type(iii), type(i)-type(iv), and type(ii)-type(iv) mode, thus yielding an MN_6, MN_5O, MN_4O_2, MN_3O_3, or MN_2O_4 coordination. This result shows that in terms of strain, the bis-taci ligand L^e should be able to form stable, hexacoordinated chelates with both oxophilic (**M14**) and nitrophilic (**M1**) metal cations. For the bis-type(i) structure **M1**, the strain energy was calculated for the parallel (*lel*) and oblique (*ob*) conformation, and it was found that the latter is slightly less stable (5 kJ mol^{-1}). The low amount of strain for the bis-type(ii) structure **M6** is remarkable, since this type of coordination is not particularly favorable for the parent M(taci) unit.[9,17] It is also noteworthy that a low-strain bis-type(iii) structure of $[M(L^e)]^{z+}$ (see **M13** in Table S1 in the Supporting Information) does not exist according to these calculations.

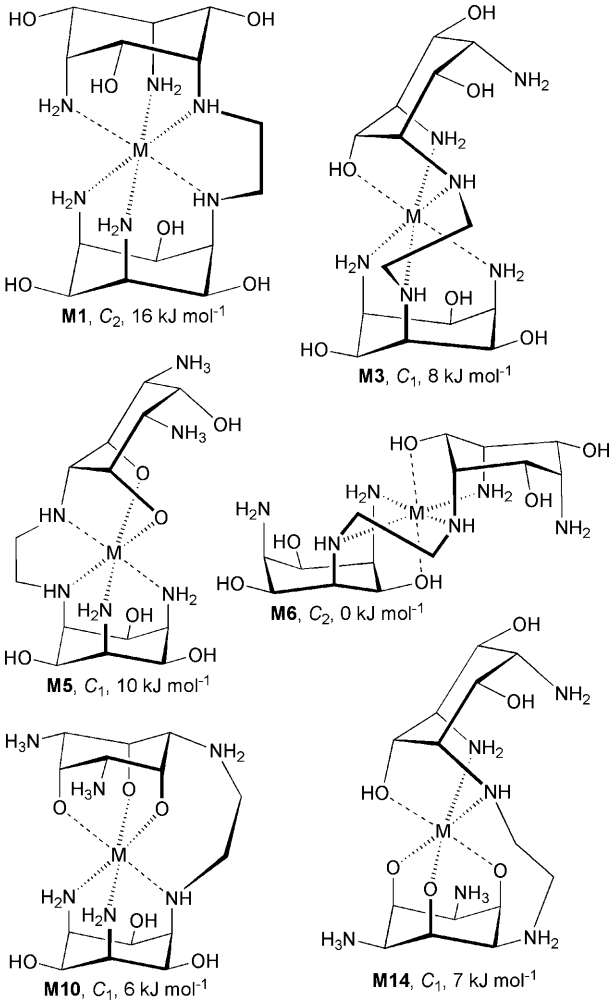

Scheme 3. Schematic representations of the six low-strain structures for a mononuclear hexacoordinated $[M(L^e)]^{z+}$ complex. The reference symbols, symmetry labels and relative total strain energies, calculated for the corresponding Co^{III} complex, are listed. A more comprehensive compilation of all 15 isomers **M1**–**M15** can be found in Table S1 in the Supporting Information.

Crystal structure of the sodium complex: A crystal of the sodium complex of composition $[Na_{0.5}(H_6L^e)](BiCl_6)_2Cl_{0.5}\cdot 4H_2O$ (**1**) was first obtained accidentally when the growth of single crystals of the free hexaprotonated ligand was envisaged. Inspection of the crystal structure of this compound revealed, however, the incorporation of some additional NaCl (Figure 3). The amount of only 0.5 equivalents is based on an examination of the electron density, exhibiting a 50% occupancy of the Na and the corresponding Cl sites, and was further confirmed by an inductively coupled plasma optical emission spectrometry (ICP-OES) analysis (yielding an occupancy of 52(2)%). Although additional NaCl (up to a 30-fold excess) was added to the test solutions in further crystallization experiments, the amount of incorporated NaCl did not increase. We explain the partial incorporation of NaCl by the large electrostatic repulsion interactions between Na^+ and $H_6(L^e)^{6+}$. The binding of Na^+ to the axial hydroxy groups of a fully protonated

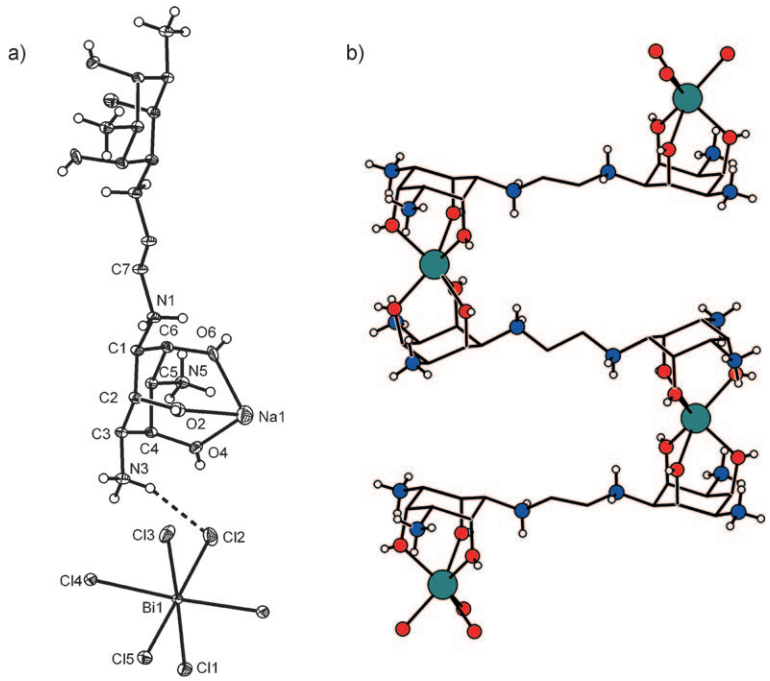

Figure 3. Structure of the Na-complex **1**: a) View of the $[Na(H_6L^e)]^{7+}$ and $[BiCl_6]^{3-}$ moieties with numbering scheme (displacement ellipsoids drawn for a 50% probability level); b) Section of the zigzag $\cdot\cdot H_6(L^e)^{6+}$-Na^+-$H_6(L^e)^{6+}\cdot\cdot$ chain structure (carbon skeleton: stick model, N: blue, O: red, Na: green spheres). The C–H-hydrogen atoms are omitted for clarity, other hydrogen atoms are shown as spheres of arbitrary size. Only half of the Na positions are occupied. Selected bond lengths [Å] and angles [°]: Na1–O2 2.298(5), Na1–O4 2.245(4), Na1–O6 2.221(4); O6-Na1-O6A 83.3(2), O6-Na1-O4A 141.7(2), O6-Na1-O4 79.51(11), O4-Na1-O4A 93.3(2), O6-Na1-O2 77.70(13), O6A-Na1-O2 129.9(2), O4-Na1-O2 79.16(12), O4A-Na1-O2 138.3(2), O2-Na1-O2A 80.0(2).

hexapositive $H_6(L^e)^{6+}$ cation is indeed a remarkable and an unexpected result. In the crystal structure, the $H_6(L^e)^{6+}$ entity is placed on a crystallographic center of inversion, generating the low-energy C_i-symmetric rotamer[11] (see Chart S1 in the Supporting Information) with an *anti*-conformation of the diaminoethane subunit. The Na^+ cations are bonded in a bis-type(iv) fashion. The hydroxy groups of the two taci subunits are thus aligned in opposite directions, forming a zig-zag chain of the type $\cdot\cdot Na^+$-$H_6(L^e)^{6+}$-Na^+-$H_6(L^e)^{6+}\cdot\cdot$. However, owing to the abovementioned disorder, only one half of the Na positions are occupied in a statistical fashion. The Na^+ ions are located on a crystallographic mirror plane and thus exhibit a coordination number of six with a strictly trigonal prismatic geometry and average Na–O distance of 2.255 Å. This value is slightly shorter than the one usually observed for a hexacoordinate Na^I.[18] Conformation analysis reveals an almost ideal chair for the cyclohexane ring (see Table S2 in the Supporting Information).[19]

The molecular structure of the Ni^{II}, Cu^{II}, Zn^{II}, and Co^{III} complex: Crystalline samples of $[Ni(L^e)]Cl_2\cdot 5H_2O$ (**2**) and $[Cu(L^e)](ClO_4)_2\cdot H_2O$ (**3**) were obtained by the simple combination of aqueous solutions of the free ligand and the corresponding metal salt followed by slow evaporation of the solvent. Single crystals of $[Zn(L^e)]CO_3\cdot 7H_2O$ (**4**) were grown from an aqueous alkaline $[Zn(L^e)](NO_3)_2$ solution after prolonged exposure to air. $[Co(L^e)]^{3+}$ was prepared by aerial oxidation of the Co^{II} complex. It was purified by cation-exchange chromatography and was isolated as a hydrated trichloride salt $[Co(L^e)]Cl_3\cdot 5H_2O$ (**5a**). For structural studies $[Co(L^e)][ZnCl_4]Cl$ (**5b**) was prepared, but the crystal structure exhibited some significant disorder for the ethylene bridge,[20] and a satisfactory description could not be performed.[21] The complex was therefore converted into the perchlorate salt $[Co(L^e)](ClO_4)_3$ (**5c**)[22] that could be more successfully used for a crystal structure analysis.

It has been previously shown that $[Ni(taci)_2]^{2+}$, $[Cu(taci)_2]^{2+}$, $[Zn(taci)_2]^{2+}$ and $[Co(taci)_2]^{3+}$ all adopt a bis-type(i) structure.[9,23–25] A corresponding hexaamine structure with L^e acting as a chelating hexaamine ligand was also observed in the crystal structures of **2**, **3**, **4**, and **5c** (Figure 4 and Figure S2 in the Supporting Information). It is noteworthy that **5c** is the only example with an *ob* orientation of the diaminoethane unit; the other hexaamine complexes adopted a *lel* orientation. The three nitrogen donors of each taci subunit define an approximately equilateral triangle. For the parent bis-taci complexes with a bis-type(i) structure a strictly trigonal antiprismatic structure has been generally observed. However, of the corresponding hexaamine $M(L^e)$ complexes, only the Co^{III} complex **5c** showed an undistorted antiprismatic geometry. For the other $M(L^e)$ complexes, some twisting towards a trigonal prismatic form was noted. The twist angle ϕ, describing the degree of distortion between a pure trigonal antiprismatic ($\phi = 60°$) and a pure trigonal prismatic ($\phi = 0°$) coordination geometry,[26] was 50.2° for the Ni complex **2**, 48.9° for the Cu complex **3**, and 48.6° for the Zn complex **4**. This observation has to be related with the geometry of the diaminoethane bridge. In contrast to the Na complex where an *anti* conformation was observed, all the hexaamine complexes exhibit a synclinal conformation with torsion N-C-C-N-angles of 56.7° (**2**), 60.8° (**3**), 60.3° (**4**) and 39.3° (**5c**). The last deviates significantly from an ideal gauche geometry. These observations indicate that the tethering of two taci fragments by an N-CH_2-CH_2-N bridge generates some additional strain that can be partially compensated, either by twisting of the two taci subunits towards a trigonal prism or by twisting the two NCH_2 fragments in the bridge from an ideal gauche towards

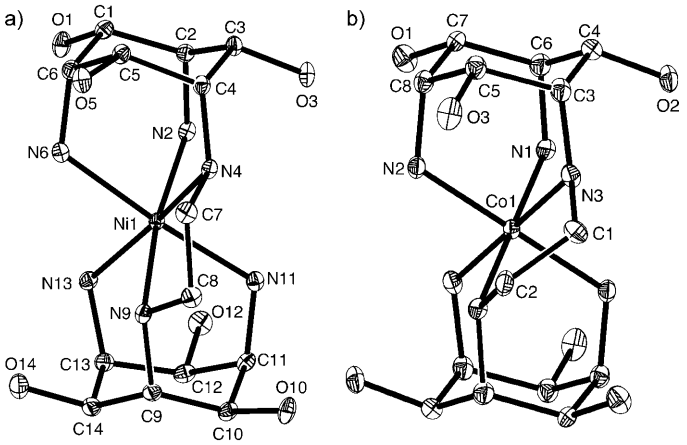

Figure 4. Molecular structures of a) $[Ni(L^e)]^{2+}$ and b) $[Co(L^e)]^{3+}$ of **2** and **5c**, respectively. Displacement ellipsoids are drawn for a 50% probability level. Hydrogen atoms are omitted for clarity. The drawings show the different orientation of the ethylene bridge (*lel* for Ni, *ob* for Co) in the two complexes. Corresponding pictures of the Cu and Zn complex are provided in Figure S2 in the Supporting Information. Selected bond lengths [Å] and angles [°], Ni-complex **2**: Ni1–N13 2.091(1), Ni1–N4 2.103(1), Ni1–N2 2.115(1), Ni1–N9 2.130(1), Ni1–N11 2.144(2), Ni1–N6 2.161(2); N13-Ni1-N4 168.49(5), N13-Ni1-N2 97.27(6), N4-Ni1-N2 92.06(5), N13-Ni1-N9 88.18(5), N4-Ni1-N9 83.36(5), N2-Ni1-N9 171.51(5), N13-Ni1-N11 91.82(6), N4-Ni1-N11 95.19(6), N2-Ni1-N11 88.34(6), N9-Ni1-N11 84.98(6), N13-Ni1-N6 88.77(6), N4-Ni1-N6 85.14(6), N2-Ni1-N6 86.08(5), N9-Ni1-N6 100.59(5), N11-Ni1-N6 174.42(5); Co-complex **5c**: Co1–N3 1.966(4), Co1–N1 1.969(4), Co1–N2 1.987(4); N1-Co1-N2 90.5(2), N3-Co1-N3A 180.0, N3-Co1-N1A 90.0(2), N3-Co1-N1 90.0(2), N1A-Co1-N1 180.0, N3-Co1-N2 88.5(2), N3A-Co1-N2 91.5(2), N1A-Co1-N2 89.5(2), N2-Co1-N2A 180.0.

an eclipsed orientation. The observed structures can be regarded as a compromise between these two effects. $[Co(L^e)]^{3+}$ with its high ligand-field stabilization exhibits a lower amount of distortion in the coordination sphere, but more twisting in the ligand backbone. For Zn^{II}, which is devoid of a ligand-field effect, the geometry of the diaminoethane bridge is almost ideal, whereas the coordination geometry is somewhat distorted towards a trigonal prism.[27] A chair conformation was observed for the cyclohexane rings of all hexaamine $M(L^e)$-complexes. However, for **2**, **3**, and **4**, a slight but significant distortion towards a half-boat (for one of the rings) or towards a half-chair (for the other ring) was noted (see Table S2 in the Supporting Information).[19] Metal–nitrogen bond lengths are as expected.[9,24,25,28] $[Cu(L^e)]^{2+}$ exhibited the usual tetragonally elongated 4+2 Jahn—Teller geometry.[29] In solution, the hexaamine structure of these complexes was retained as indicated by the UV/Vis parameters for $[Co(L^e)]^{3+}$ ($\lambda_{max}=340$ and 471 nm), $[Ni(L^e)]^{2+}$ ($\lambda_{max}=321$, 511 and 799 nm) and $[Cu(L^e)]^{2+}$ ($\lambda_{max}=603$ nm), and the NMR characteristics of $[Co(L^e)]^{3+}$. The ^{13}C NMR and the ^{1}H NMR spectra exhibited six and eight resonances,[30] respectively, with two separate signals for the CH_2 hydrogen atoms of the ethylene bridge, indicating a chiral C_2 symmetry for the solution structure. In contrast to the labile Ni^{II}, Cu^{II} and Zn^{II} complexes, that readily decay in acidic media (vide infra), the inert hexaamine structure of $[Co(L^e)]^{3+}$ is, as expected, unaffected for prolonged periods of time even in 6 M HCl.

Molecular structure of $[Ga(H_{-2}L^e)]^+$: Single crystals of a colorless Ga^{III} complex of composition $[Ga(H_{-2}L^e)]NO_3\cdot 2H_2O$ (**6**) were obtained by slow evaporation of an aqueous solution that was obtained by the simple combination of $Ga(NO_3)_3$ and L^e. Although the ligand L^e coordinates as the doubly deprotonated anion $(H_{-2}L^e)^{2-}$, addition of base to the reaction mixture was not necessary. A single-crystal X-ray analysis revealed a bis-type(ii) structure of the complex cation (**M6** in Scheme 3) with a *trans*-GaN_4O_2 coordination (Figure 5). In the crystal structure, the $[Ga(H_{-2}L^e)]^+$ cation is placed on a general position and is thus devoid of any crystallographically imposed symmetry. However, deviation from C_2 symmetry is not significant; a pseudo twofold rotational axis is running through the Ga center and the center of the ethylene bridge. It is noteworthy that the parent bis-taci complex $[Ga(taci)_2]^{3+}$ adopted a type(i)-type(iv) structure with a mixed GaN_3O_3 coordination.[31] As shown in Scheme 3, the corresponding zwitterionic bis-adamantane-$[Ga(L^e)]^{3+}$ isomer **M10** would also belong to the low-strain structures. However, the bis-type(ii) coordination **M6** is even less strained, and deprotonation of the two oxygen donors would result in a further release of strain. The adoption of this low-strain structure is apparently one of the driving forces for this particular geometry. The Ga–N and Ga–O bond distances in $[Ga(H_{-2}L^e)]^+$ and $[Ga(taci)_2]^{3+}$ are in close agreement.

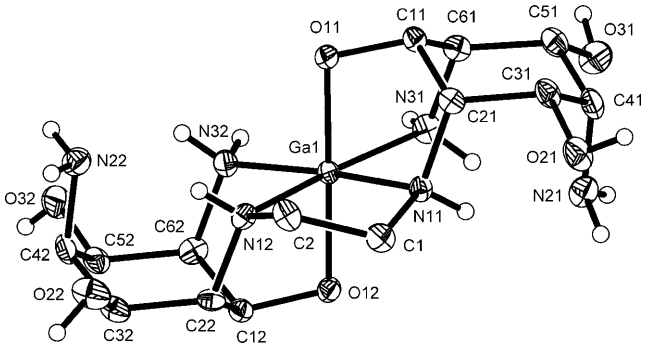

Figure 5. Molecular structure of $[Ga(H_{-2}L^e)]^+$ of **6**. Displacement ellipsoids are drawn for a 30% probability level. H–O and H–N hydrogen atoms are shown as spheres of arbitrary size; H–C hydrogen atoms are omitted for clarity. Selected bond lengths [Å] and angles [°]: Ga1–O11 1.942(3), Ga1–O12 1.947(4), Ga1–N11 2.119(4), Ga1–N12 2.085(4), Ga1–N31 2.077(4), Ga1–N32 2.061(4); O11-Ga1-O12 177.2(2), O11-Ga1-N32 97.8(2), O12-Ga1-N32 83.5(2), O11-Ga1-N31 84.2(2), O12-Ga1-N31 98.0(2), N32-Ga1-N31 102.9(2), O11-Ga1-N12 93.9(2), O12-Ga1-N12 83.7(2), N32-Ga1-N12 86.2(2), N31-Ga1-N12 170.9(2), O11-Ga1-N11 83.0(2), O12-Ga1-N11 95.4(2), N32-Ga1-N11 171.2(2), N31-Ga1-N11 86.0(2), N12-Ga1-N11 85.0(2).

Hydrogen bonding: Owing to the high number of amino and hydroxy groups of the ligand L^e, hydrogen bonding is one of the principal structural motives in the crystal structures of **1**–**6**. The N–H hydrogen atoms of the ammonium groups of **1** and the N–H hydrogen atoms of the coordinated amino groups of **2**–**6** generally act as hydrogen donors; also the coordinated hydroxy groups of **1** serve exclusively as hydrogen donors, whereas the non-coordinated hydroxy groups of **2**–**6**, as well as the water molecules, serve as hydrogen donors and hydrogen acceptors. The two coordinated alkoxo oxygen groups of **6** act as strong hydrogen acceptors, and the non-coordinated primary amino groups of **6** accept an N–H hydrogen atom of the coordinated amino groups by intra-molecular hydrogen bonding. This type of intra-molecular hydrogen bond formation is well established for the type(ii) coordination mode.[9,17] Some of the counter anions are also involved as hydrogen acceptors in the hydrogen bonding networks. A complete overview of the explicit hydrogen bond interactions in **1**–**6** is given as supporting information (Table S3).

Formation constants: The formation constants of L^e with Mn^{II}, Cu^{II}, Zn^{II}, and Cd^{II} were determined in aqueous media by potentiometric titrations. For all metal cations, a large variety of species of general composition $[M_x(L^e)_yH_z]^{2x+z}$ had to be taken into account. As a matter of fact, the selection of a proper and unambiguous speciation model proved to be difficult, because the analysis of one single titration curve often allowed the assignment of more than one set of species with a similar goodness of fit. In terms of a case study, we will describe here the treatment of the Cu^{II}-L^e system in detail. This system is particularly suited for such an investigation, since the potentiometric study can be combined with spectrophotometric measurements. For this purpose, the titration cell was equipped with an immersion probe, connected to a diode array spectrophotometer, allowing the recording of spectra during the titration (Figure 6a). The UV/Vis data of the blue Cu^{II}-complexes provided valuable independent information that could be used to corroborate the validity and accuracy of the selected model (Table 2). The additional data also allowed the calculation of individual spectra (Figure 6b) for each species, which could be used for structural assignments (Scheme 4).[32] In a first step, a set of 12 titration curves were used for the evaluation with sample solutions having total Cu to total ligand ratios of 1:1 and 2:1. In the 2:1 solutions, dinuclear species $[Cu_2(L^e)H_z]^{4+z}$ $(0 \geq z \geq -3)$ strongly predominate above pH 5, and a first estimate for their formation constants could be obtained. The titration experiments with the 1:1 solutions were evaluated with the previously determined constants of the dinuclear species treated as fixed values, yielding a set of constants for mononuclear species $[Cu(L^e)H_z]^{2+z}$ $(-1 \leq z \leq 3)$. Finally, all 12 titration curves were combined into one single data set for a last concluding evaluation. In this final evaluation the formation constants of all metal containing species were simultaneously refined. Additional titrations with sample solutions where the ligand was present in excess have then been performed. They were consistent with the previous results and did not provide evi-

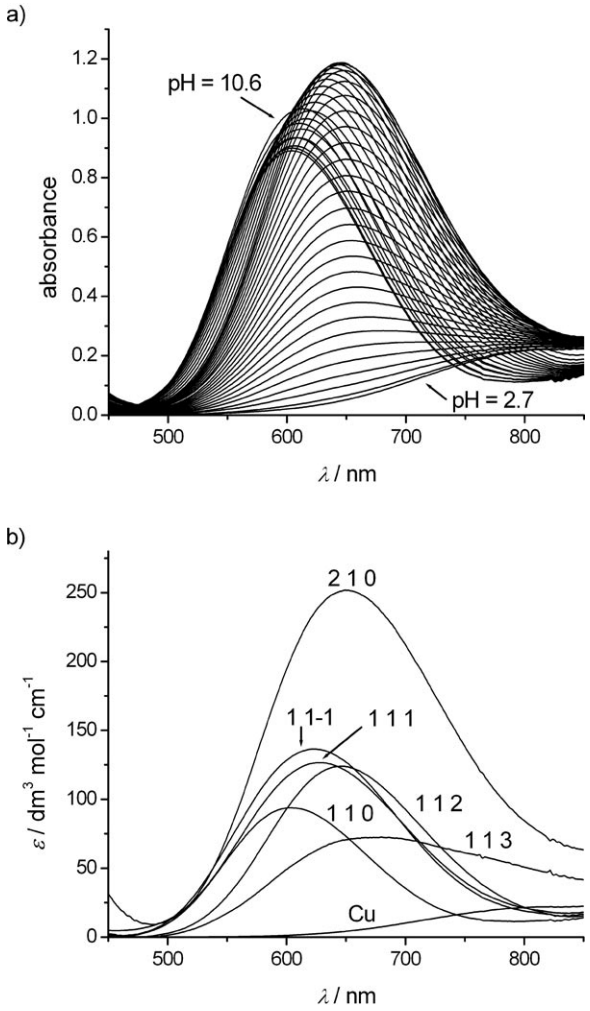

Figure 6. a) Spectral changes for the Cu^{II}-L^e system during a titration experiment with equimolar concentrations (10 mM) of total Cu and total L^e (1 M KCl, 25 °C). b) The calculated spectra for the individual species of composition $Cu_xL^e_yH_z$ (labeled as xyz). The spectrum of Cu^{II} was measured separately and kept constant in the refinement.

Table 2. Summary of the evaluated formation constants of the Cu^{II}-(L^e) system (25 °C, inert electrolyte as indicated) with estimated uncertainties (3σ) in parentheses. Values are shown for the evaluation of the potentiometric (pot) and spectrophotometric (spec) titrations.

$\log\beta_{xyz}$[a]	0.1 M KCl		1.0 M KCl		1.0 M KNO_3
	pot	spec[b]	pot	spec[c]	pot
$\log\beta_{110}$	20.11(2)		19.85(2)	19.80(2)	20.56(1)
$\log\beta_{111}$	25.64(2)		25.72(2)	25.57(2)	26.36(1)
$\log\beta_{112}$	30.46(1)	30.49(2)	31.04(2)	30.97(2)	31.56(1)
$\log\beta_{113}$	33.23(6)		33.95(6)	34.05(4)	34.30(3)
$\log\beta_{11-1}$	9.86(3)		9.36(3)	9.41(3)	
$\log\beta_{210}$	26.09(2)	26.12(4)	26.23(5)	26.30(2)	26.42(7)
$\log\beta_{21-1}$	19.82(3)	19.54(4)			
$\log\beta_{21-2}$	13.16(2)	13.52(6)			
$\log\beta_{21-3}$	2.11(3)				

[a] $\beta_{xyz} = [Cu_x(L^e)_yH_z] \times [Cu]^{-x} \times [(L^e)]^{-y} \times [H]^{-z}$. [b] Measured for total Cu = 2 mM, total L^e = 1 mM. [c] Measured for total Cu and total L^e = 10 mM.

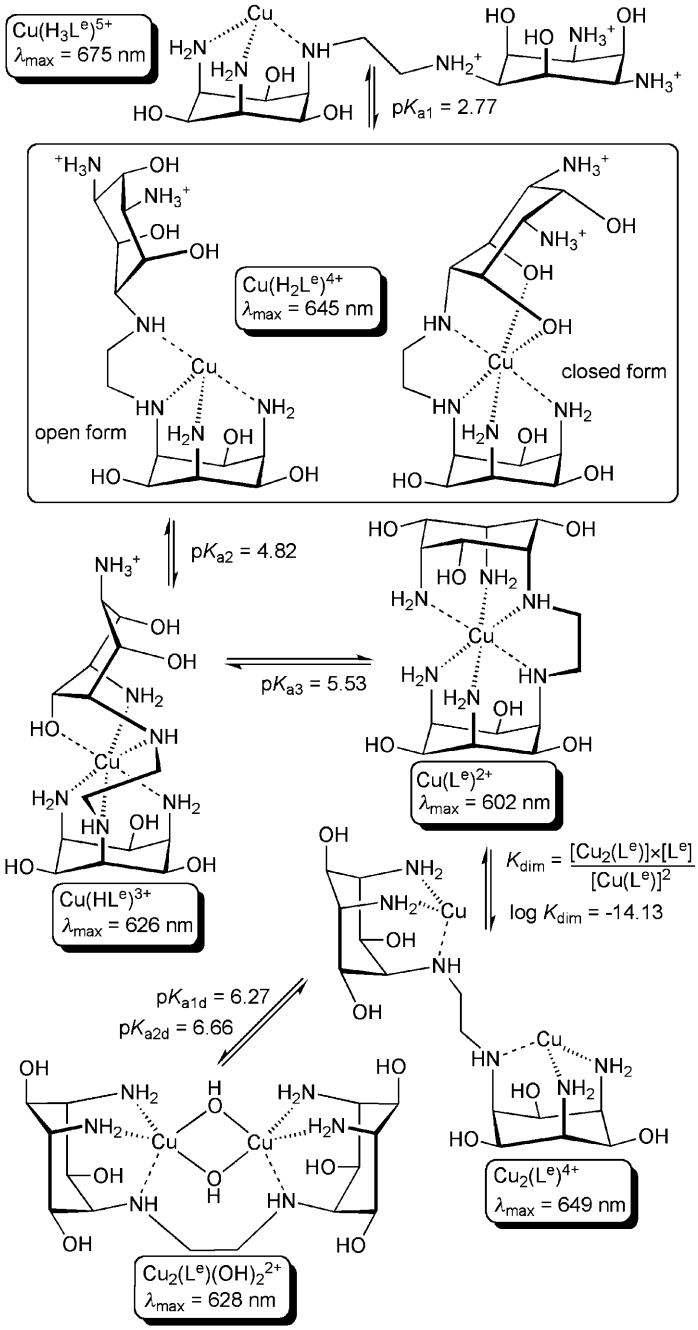

Scheme 4. Possible structures for the various Cu^{II} complexes formed in aqueous solution. Only the Cu-L^e moieties are depicted, additional water molecules which may be coordinated to the Cu centers are omitted for clarity.

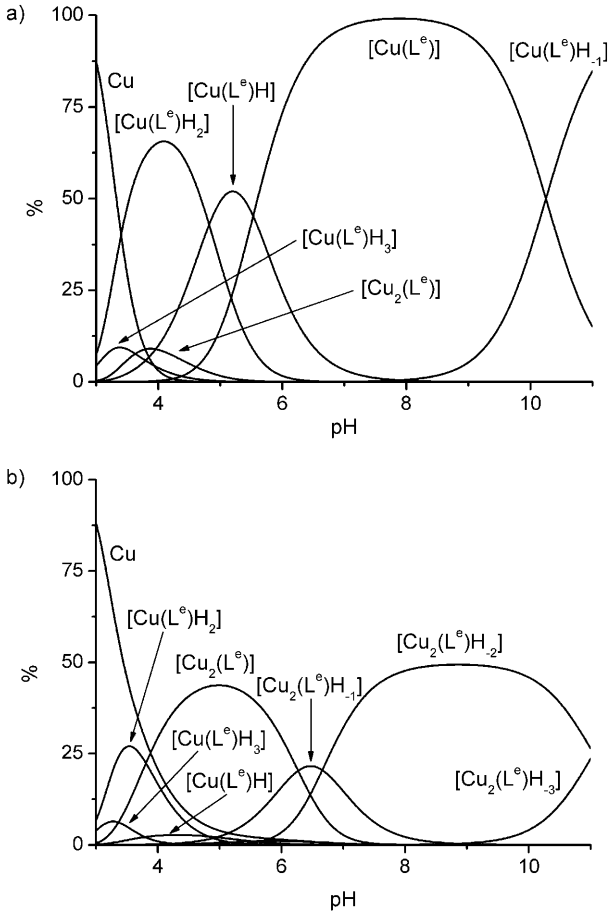

Figure 7. pH-dependent species distribution plot for the Cu^{II}-L^e system a) with equal total concentrations (1 mM) of Cu and L^e, b) with excess Cu (total L^e = 1 mM, total Cu = 2 mM). The distributions were calculated using the formation constants listed in Table 2 (0.1 M KCl). The percentage refers to the abundance of each species; that is, the amount of Cu is twice the one shown for dinuclear complexes. Charges are omitted for clarity; possible structures of the Cu^{II} complexes are shown in Scheme 4.

dence for the formation of further species with more than one ligand entity ($y > 1$).

Species distribution plots for the Cu^{II}-L^e system are shown in Figure 7. For equimolar concentrations of L^e and Cu^{II}, complex formation starts around pH 3. At this pH a small amount of the triply protonated $[Cu(L^e)H_3]^{5+}$ (λ_{max} = 675 nm) is formed. Stepwise deprotonation leads to $[Cu(L^e)H_2]^{4+}$ (λ_{max} = 645 nm), $[Cu(L^e)H]^{3+}$ (λ_{max} = 626 nm), $[Cu(L^e)]^{2+}$ (λ_{max} = 602 nm), and $[Cu(L^e)H_{-1}]^{+}$ (λ_{max} = 618 nm). The uncharged doubly deprotonated $[Cu(L^e)H_{-2}]$ is only observed as a minor species at high pH (the pK_a of $[Cu(L^e)H_{-1}]^{+}$ is > 12). Only one dinuclear complex, $[Cu_2(L^e)]^{4+}$ (λ_{max} = 649 nm), appears to a minor degree around pH 4. Based on the λ_{max} value of 675 nm, we assigned a mono-type(i) structure to the triply protonated $[Cu(L^e)H_3]^{5+}$ with the other taci subunit remaining protonated;[16,32] this assignment is in agreement with λ_{max} = 683 and 658 nm observed for the corresponding *facial* Cu^{II}-triamine chromophore of $[Cu(tach)]^{2+}$ and $[Cu(tacn)]^{2+}$, respectively.[6,33] The observed monotonic shift of λ_{max} to lower values indicates that the progressive deprotonation of $[Cu(L^e)H_3]^{5+}$ is coupled with a coordination of further nitrogen donors. Such a conclusion is also supported by the relatively low values of the apparent pK_a values of $[Cu(L^e)H_3]^{5+}$ (2.77, 4.82, 5.53) that are lower than the pK_a values of the fully protonated $H_6(L^e)^{6+}$. It should be noted that a λ_{max} = 645 nm, observed for $[Cu(L^e)H_2]^{4+}$ (which will receive a tetraamine coordination according to these considerations), is only compatible with a *cis*-CuN_4O_2 configuration; the *trans*

configuration with four nitrogen donors in the equatorial positions of an elongated octahedron would absorb in the range of 540–580 nm.[32,34,35] A bis-type(ii) mode (i.e. a doubly protonated structure of **M6** in Scheme 3) can thus be excluded for this particular complex. The value of $\lambda_{max}=$ 602 nm, calculated for $[Cu(L^e)]^{2+}$ is in close agreement with $\lambda_{max}=603$ nm observed for a solution of a crystalline sample of **3**. $[Cu(tach)_2]^{2+}$ absorbs at $\lambda_{max}=635$ nm and $[Cu(dapi)_2]^{2+}$ at 614 nm (dapi = *cis*-3,5-diaminopiperidine).[6,15] Obviously, the presence of two secondary nitrogen donors results in some increase of the ligand field. The dinuclear $[Cu_2(L^e)]^{4+}$ exhibited a λ_{max} of 649 nm. For the proposed facial type(i) coordination, this value is relatively low. It compares, however, very well with $\lambda_{max}=647$ nm, reported by Mancin et al. for a related dinuclear species of the bis-taci ligands L^{mx} and L^{px} , which have a *meta*- or *para*-xylene linker, respectively.[7] Above pH 5, deprotonation of $[Cu_2(L^e)]^{4+}$ yields $[Cu_2(L^e)H_{-1}]^{3+}$ and $[Cu_2(L^e)H_{-2}]^{2+}$ (Figure 7b). The apparent pK_a values are 6.27(3) and 6.66(3). The relatively low numbers (particularly for the second deprotonation step) can be explained by an additional stabilization due to Cu-OH-Cu bridging (Scheme 4).[7]

The formation constant of $[Cu(L^e)]^{2+}$ ($\log\beta=20.11$) is only slightly higher than the formation constant of the parent $[Cu(taci)_2]^{2+}$ ($\log\beta_2=18.79$).[24] Thus it appears that the chelate effect of the hexadentate ligand is partially outweighed by the additional strain within the CuL^e-structure. Comparison with other hexaamine analogues confirmed that the $[Cu(L^e)]^{2+}$-complex is not of particularly high stability (Table 3). This is true not only for the mononuclear, but also for dinuclear species, such as $[Cu_2(L^e)]^{4+}$.[36] The comparably low stability can thus not only be attributed to the strain introduced by the ethylene bridge. It also seems to be a result of the reduced nucleophilicity of the amino groups of L^e, caused by the electron-withdrawing properties of the additional hydroxy groups. However, the electron-withdrawing effect also reduces basicity, and in terms of conditional stability, L^e is an effective chelator in slightly acidic and neutral media.

Table 3. Formation constants $\log\beta_{ML}$[a] for the bis-taci ligand (L^e) in comparison with some other hexaamine ligands previously reported in the literature.[b,c]

	Mn^{II}	Cu^{II}	Zn^{II}	Cd^{II}
L^e[d]	6.13(3)	20.11(2)	13.60(2)	10.43(2)
L^{mx}[e]	–	–	7.75	–
L^{px}[e]	–	–	8.05	–
penten[f]	9.24	22.15	16.15	16.15
3,2,2,2,3-hex[g]	–	21.74	14.45	–
3,3,2,3,3-hex[h]	–	19.35	10.53	9.46
[18]aneN6[i]	10.50	24.40	18.70	18.80
bis-tacn[j]	–	27.82	–	–

[a] $\beta_{ML}=[ML]\times[M]^{-1}\times[L]^{-1}$. [b] Reference [37], unless otherwise noted. [c] 25 °C, $\mu=0.10$ M, unless otherwise noted. [d] This work; estimated uncertainties (3σ) in parentheses. [e] Systematic names: see section: preparation and characterization of the ligand, data from reference [7]. [f] 4,7-Bis(2-aminoethyl)-1,4,7,10-tetraazadecane. [g] 1,5,8,11,14,18-Hexaazaoctadecane; 25 °C, 0.15 M $NaClO_4$. [h] 1,5,9,12,16,20-Hexaazaicosane; 25 °C, 0.15 M $NaClO_4$. [i] 1,4,7,10,13,16-Hexaazacyclooctadecane. [j] 1,2-Di(1,4,7-triazonan-1-yl)ethane.

In solutions containing an equimolar ratio of Zn^{II} and L^e, the mononuclear $[Zn(L^e)]^{2+}$ is the predominant species around pH 7 ($\log\beta_{110}=13.6$). At lower pH, a series of protonation products $[Zn(H_xL^e)]^{2+x}$ is formed. The Cd–L^e-system behaves similarly ($\log\beta_{110}=10.4$). A complete list of the evaluated formation constants together with some structural representations of the complexes are provided in the Supporting Information (Table S4 and Chart S2). It is noteworthy that for Zn^{II} and Cd^{II}, the maximum amount of protonation ($x=5$) is higher than for Cu^{II} ($x=3$). In $[M(H_5L^e)]^{7+}$ only one amino group can be coordinated to the metal ion, and for electrostatic reasons, the $H_5(L^e)^{5+}$ unit probably adopts a chair conformation with equatorial nitrogen atoms. Additional coordination of the metal cation to two axial hydroxy groups by a type(iii) binding is feasible. The individual formation constants $\log K_i$ of 2.27 (Zn) and 2.67 (Cd), expressed by the reaction $H_5(L^e)^{5+}+M^{2+}=M(H_5L^e)^{7+}$, $K_i=[M(H_5L^e)^{7+}]\times[H_5(L^e)^{5+}]^{-1}\times[M^{2+}]^{-1}$, compare well with the stability ($\log\beta_1$) of the corresponding monoammine complexes $M(NH_3)^{2+}$, which are reported to be 2.3 and 2.62, respectively.[39] In the course of deprotonation of $M(H_5L^e)^{7+}$, a chair conversion must occur and this conformational change possibly explains the non-observance of the partially protonated complexes $[Zn(H_4L^e)]^{6+}$ and $[Cd(H_2L^e)]^{4+}$. A further interesting difference to the Cu^{II}-L^e-

A final comment should be made on the difference of the formation constants in a 1.0 M KCl and 1.0 M KNO_3 medium. In the chloride medium, the formation constants are generally smaller, which is indicative of chloro complex formation. Assuming negligible $NO_3^-\cdots Cu^{2+}$ interactions, we have calculated a value of 0.58(2) for $\log K$ of the reaction $Cu^{2+}+Cl^-=CuCl^+$. For the series $[Cu(H_xL^e)]^{2+x}+Cl^-=[Cu(H_xL^e)Cl]^{1+x}$, we have found $\log K$ values of $-0.07(3)$ for $x=2$, $+0.35(7)$ for $x=3$, and $+1.34(5)$ for the dinuclear species, that is, for $[Cu_2(L^e)]^{4+}+Cl^-=[Cu_2(L^e)Cl]^{3+}$. Interestingly, no significant chloride binding was observed for $[Cu(L^e)]^{2+}$ and $[Cu(HL^e)]^{3+}$, an observation that further supports the hexacoordinated structures shown in Scheme 4. The significant chloride binding of $[Cu(H_2L^e)]^{4+}$ provides evidence for an open rather than a closed structure of this particular complex (see box in Scheme 4).

Complex formation of L^e with Mn^{II} is generally weak. Significant metal binding was only observed above pH 7. At these conditions, the sample solutions proved to be highly sensitive towards oxidation, especially when the metal cation was present in excess. The formation constant of $[Mn(L^e)]^{2+}$ could be established ($\log\beta=6.1$, see Table 3), but an unambiguous verification of dinuclear species, such as $[Mn_2(L^e)]^{4+}$, was not possible. Protonated species of composition $[Mn(L^e)H_x]^{2+x}$ play, if at all, only a minor role. The weak tendency of L^e to bind to Mn^{II} coincides with the low stability of the corresponding taci complexes ($\log\beta_{110}=4.0$, $\log\beta_{120}<7$).[38]

system is the non-observance of the dinuclear $[M_2(L^e)]^{4+}$. Titration experiments with a total metal to total ligand ratio of 2:1 unambiguously established that Zn^{II} and Cd^{II} do not form such a species under the conditions employed (see Figure S3 in the Supporting Information). In solutions with an excess of the metal cation, we observed, however, formation of trinuclear complexes of composition $[M_3(L^e)_2]^{6+}$ together with corresponding deprotonation products. Moreover, if the ligand is applied in excess, the formation of additional components can be observed. For Zn, we have not yet succeeded in establishing a conclusive model for explaining the experimental data. However, for Cd the potentiometric data are in excellent agreement, assuming formation of a series of dinuclear species of composition $[Cd_2(L^e)_3H_x]^{4+x}$ (see Table S4 and Chart S2 in the Supporting Information).

Our findings for the Zn^{II}–L^e system differ from the observations of Mancin et al., who observed mononuclear $[Zn(L^{mx})]^{2+}$ and $[Zn(L^{px})]^{2+}$ complexes with a remarkably low stability of $\log\beta_{110}=7.75$ and 8.05, respectively.[7] These values rather correspond to $\log\beta_{110}=8.40$, observed for $[Zn(taci)]^{2+}$,[24] thus indicating tridentate coordination. Obviously the rigidity of the xylene bridge impedes a hexadentate chelation of L^{mx} and L^{px}. Mancin et al. also reported formation of the dinuclear $[Zn_2(L^{mx})]^{4+}$ and $[Zn_2(L^{px})]^{4+}$, whereas in our study such species could not be observed (vide supra). This latter difference between the ethylene- and the xylene-bridged ligands is obviously less trivial.

The lower stability of $[Cd(L^e)]^{2+}$compared to $[Zn(L^e)]^{2+}$ is in accordance with the behavior of the corresponding taci complexes.[40] In general, the stability of ML^e complexes can be well reproduced by linear free energy relations, such as Equations (1)–(4) with correlation coefficients of 0.999 or higher (Figure 8).

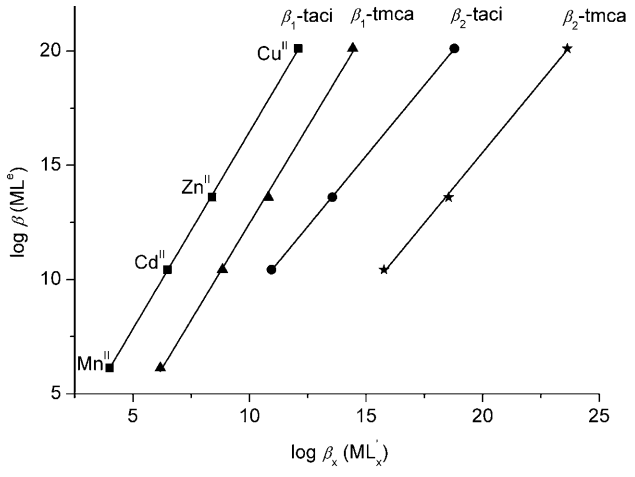

Figure 8. Graphical representations of the Linear-free-energy relations $\log\beta(ML^e)=a\cdot\log\beta_x(ML'_x)-b$, L′ = taci or tmca, $x=1$ or 2, as listed in the Equations (1)–(4) discussed in the text (taci = 1,3,5-triamino-1,3,5-trideoxy-*cis*-inositol, tmca = *all-cis*-2,4,6-trimethoxycyclohexane-1,3,5-triamine). The formation constants of the taci and tmca complexes are from references [13], [24], [38], and [40].

$$\log\beta_{ML^e}=1.73(1)\cdot\log\beta_{M(taci)}-0.8(1) \quad (1)$$

$$\log\beta_{ML^e}=1.24(1)\cdot\log\beta_{M(tmca)_2}-3.1(1) \quad (2)$$

$$\log\beta_{ML^e}=1.69(4)\cdot\log\beta_{M(tmca)}-4.5(4) \quad (3)$$

$$\log\beta_{ML^e}=1.24(3)\cdot\log\beta_{M(tmca)_2}-9.2(7) \quad (4)$$

Redox properties: The redox behavior of the Mn, Ni and Co complexes was investigated in aqueous media by cyclic voltammetry. The free ligand L^e was found to be redox-inactive over the entire pH range. Cyclic voltammograms of $[Ni(L^e)]^{3+/2+}$ and $[Co(L^e)]^{3+/2+}$ exhibited quasi-reversible redox behavior in the range $7<pH<10$ with redox potentials of $+0.90$ V and -0.38 V vs. NHE, respectively. Similar potentials have been observed for $[Ni(taci)_2]^{3+/2+}$ and $[Ni(tmca)_2]^{3+/2+}$ (both 0.97 V), $[Co(taci)_2]^{3+/2+}$ (-0.39 V), and $[Co(tmca)_2]^{3+/2+}$ (-0.36 V).[15] The potentials observed did not depend on pH, but, in acidic solutions, an irreversible reaction was observed attributed to the decay of the complexes in the divalent stage. The peak separations were 76 and 68 mV, respectively (pH 9, scan rate of 10 mVs^{-1}). A strictly linear dependence of the peak current on the square root of the scan rate was observed for both systems, as expected for a diffusion-controlled process. All these observations confirm the presence of a mononuclear hexaamine complex in solution, as observed in the corresponding crystal structures **2** and **5c**. Also the Mn-L^e system displayed redox activity in aqueous alkaline media. However, cyclic voltammetry exhibited a strongly irreversible behavior and an unambiguous assignment of the corresponding electron transfer processes was not possible.

Conclusion and Outlook

The potentially hexadentate, ethylene-bridged bis-taci ligand L^e offers the possibility of mononuclear hexacoordinate chelation or metal bridging. In this paper, we provided ample evidence for both types of interactions. Formation of mononuclear chelates in the solid state could be characterized for Co^{III}, Ni^{II}, Cu^{II}, Zn^{II}, and Ga^{III} by crystal-structure analyses. An extended solution study verified that such species were also formed in dilute solution, provided that an equimolar ligand to metal ratio is applied. However, as exemplified for Cu^{II}, the chemistry of such solutions is much more diverse, comprising formation of a series of partially protonated $[Cu(L^e)H_x]^{2+x}$ species in equilibrium with the dinuclear $[Cu_2(L^e)]^{4+}$. If the metal cation is present in excess, the dinuclear $[Cu_2(L^e)]^{4+}$ becomes the predominant species. We tentatively assign binding of each of the two Cu^{II} centers to one of the two taci subunits resulting in a *fac*-CuN_3-coordination. The dinuclear as well as the protonated species deserve additional interest as possible catalysts for the hydrolysis of biopolymers.[7,41] For Zn^{II} and Cd^{II} formation of a $[M_2(L^e)]^{4+}$ dimer was not observed. The two cations form, however, trimeric aggregates, which can be regarded as a

starting point for the formation of 1D polymers. The binding of more than one metal cation to L^e also opens interesting possibilities for the design of extended frameworks in the solid state.[42] The Na complex **1** is a first example for this type of structure. Moreover, this complex is remarkable because of the coordination of the Na^+ ion to the fully hexaprotonated $H_6(L^e)^{6+}$. Considering the significant electrostatic repulsion between the cation and the ligand, the formation of such a structure is far from trivial. In this sodium complex, the cation is bonded to the hydroxy groups of L^e, and the interplay O versus N coordination is a further fascinating aspect of this molecule. As demonstrated by the molecular mechanics study, the question which type of structure will be adopted by a metal cation may be less evident than expected at a first glance. Late transition metal cations with their high affinity for nitrogen donors exhibit a hexaamine structure in their mononuclear stage. However, the Ga complex **6** is an example which demonstrates that further coordination modes must also be taken into account. The observed **M6** structure also demonstrates that with regard to the coordination mode, a simple extrapolation from $M(taci)_2$ to ML^e is not always conclusive.

Experimental Section

General: Commercially available chemicals used for the synthetic work were of reagent grade quality. Unless otherwise noted, chemicals were used as obtained. Dowex 50W-X2 (H^+ form) and Dowex 2-X8 (Cl^- form) were from Sigma Aldrich. The anion exchange resin was converted into the OH^- form by elution with 0.3 M aqueous NaOH and extensive rinsing with H_2O until a neutral eluent was obtained. For the potentiometric and spectrophotometric titrations, metal salts of the highest available quality (>99.95%) were used. H_2O was distilled twice (quartz apparatus). UV/Vis spectra of individual samples were measured by using an Uvikon 941 spectrometer (H_2O, 25±3°C). IR spectra were recorded by using a Bruker Vector 22 FT IR spectrometer equipped with a Golden Gate ATR unit. ^1H and ^{13}C NMR spectra were measured in $CDCl_3$ or D_2O at 21°C by using a Bruker DRX Avance 400 MHz NMR spectrometer (resonance frequencies: 400.13 MHz for ^1H and 100.6 MHz for ^{13}C). The 2D spectrum displayed in Figure 1 was performed as a gradient-selected (gs) ^1H–^{13}C HMBC experiment. Chemical shifts are given relative to [D_4]sodium (trimethylsilyl)propionate (D_2O) or tetramethylsilane ($CDCl_3$) as internal standards ($\delta=0$ ppm); m′ denotes broad unresolved multiplets. C, H, N analyses were performed by H. Feuerhake and A. Zaschka (Universität des Saarlandes); the Na and Bi analyses (ICP-OES) were performed by T. Allgayer (Universität des Saarlandes).

***all-cis*-2,4,6-Tris(benzyloxy)-1,3,5-cyclohexanetriamine (P1)**:[13] [Ni(taci)$_2$]$SO_4\cdot 4H_2O$[23] (5.0 g, 8.6 mmol) was suspended in DMF (400 mL). NaOH (11.8 g, 0.295 mol) and benzylbromide (35 mL, 0.295 mol) were added, and the reaction mixture was stirred for 24 h at room temperature. Concentrated ammonia (10 mL) was added to destroy the excess benzylbromide. The reaction mixture was stirred for 30 min, and H_2O (1.5 L) was then added. Precipitation was observed. The suspension was allowed to stand at 0°C for 10 h. The pink residue was filtered off and washed twice with H_2O (100 mL). The solid was dissolved in EtOH, and the free trihydrochloride was precipitated by addition of aqueous conc. HCl (100 mL). The suspension was allowed to stand at 0°C for another 10 h. The white residue was then filtered off and dissolved in H_2O (150 mL). An excess of NaOH (10 mL of a 40% aqueous solution) was added, and the resulting free triamine was extracted with $CHCl_3$. The organic solution was evaporated to dryness under reduced pressure, and the resulting white solid was dried in vacuo for 24 h. Yield: 6.0 g (13.4 mmol, 78%). ^1H NMR ($CDCl_3$): $\delta=2.92$ (s, 6H), 3.19 (t, $J=4$ Hz, 3H), 3.77 (t, $J=4$ Hz, 3H), 4.67 (s, 6H), 7.37 ppm (m, 15H); ^{13}C NMR ($CDCl_3$): $\delta=51.8$, 70.3, 75.1, 127.7, 127.8, 128.4, 137.8 ppm; IR: $\tilde{\nu}=608$, 641, 697, 734, 910, 1029, 1070, 1209, 1286, 1391, 1453, 1495, 1585, 2873, 3027, 3386 cm^{-1}; elemental analysis calcd (%) for $C_{27}H_{33}N_3O_3$ (447.57): C 72.46, H 7.43, N 9.39; found: C 72.10, H 7.37, N 9.27.

***N*-[6,8,9-Tris(benzyloxy)-3-oxo-2,4-diazabicyclo[3.3.1]non-7-yl]acetamide (P2)**:[10] The triamine **P1** (9.0 g, 20 mmol) was dissolved in $CHCl_3$ (120 mL, purified prior to use by column chromatography over alumina to remove traces of EtOH). Under an atmosphere of N_2, 1,1′-carbonyldiimidazole (3.36 g, 21 mmol) was added. The solution was stirred for 30 min, and AcOAc (5.82 mL, 61.6 mmol) was added. The solution was stirred for another 120 min. The solvent was then removed under reduced pressure and the residue was dissolved in CH_2Cl_2 (50 mL). The organic layer was washed twice with 1 M NaOH (100 mL) and 1 M HCl (100 mL) and was then evaporated to dryness. The solid was dried in vacuo for 24 h. It was dissolved in CH_2Cl_2 (50 mL) and purified by column chromatography (SiO_2, EtOAc/MeOH 8:1). The solvent of the main fraction was then removed under reduced pressure and the resulting solid was dried in vacuo to yield a white voluminous powder of the amide **P2** (9.85 g, 19.1 mmol, 96%). ^1H NMR ($CDCl_3$): $\delta=1.96$ (s, 3H), 3.29 (m, 3H), 3.76 (m′, 2H), 4.42 (d, $J=12$ Hz, 2H), 4.46 (s, 2H), 4.68 (d, $J=12$ Hz, 2H), 5.15 (m, 1H), 5.97 (d, $J=10$ Hz; NH), 6.62 (m′, 2NH), 7.21–7.34 ppm (m, 15H); ^{13}C NMR ($CDCl_3$): $\delta=23.5$, 45.0, 52.9, 65.5, 70.0, 70.9, 74.6, 127.7, 127.8, 128.0, 128.2, 128.6, 128.7, 136.5, 137.1, 156.4, 171.7 ppm; IR: $\tilde{\nu}=601$, 696, 869, 912, 1025, 1074, 1228, 1276, 1312, 1360, 1453, 1495, 1667, 2358, 2866, 3061, 3325, 3447 cm^{-1}; elemental analysis calcd (%) for $C_{30}H_{33}N_3O_5$ (515.60): C 69.88, H 6.45, N 8.15; found: C 68.94, H 6.48, N 7.74.

7-Amino-6,8,9-trihydroxy-2,4-diazabicyclo[3.3.1]nonan-3-one (P3): The amide **P2** (10 g, 19.4 mmol) was dissolved in 6 M aqueous HCl (500 mL) and refluxed for 3 h. The reaction mixture was concentrated to a total volume of 100 mL and allowed to cool to 25°C. The resulting solution was extracted twice with Et_2O (100 mL). The aqueous layer was evaporated to dryness and dried in vacuo for 48 h to give the amine as the hydrochloride **P3**$\cdot$HCl$\cdot 2H_2O$ (white powder, 5.24 g, 19.0 mmol, 98%). ^1H NMR (D_2O, pH*<2):[43] $\delta=3.73$ (m, 2H), 3.81 (t, $J=6$ Hz, 1H), 3.93 (t, $J=2.5$ Hz, 1H), 4.10 ppm (dd, $J_1=2.5$, $J_2=6$ Hz, 2H); ^{13}C NMR (D_2O, pH*<2):[43] $\delta=55.3$, 58.2, 61.7, 68.8, 159.9 ppm; IR: $\tilde{\nu}=709$, 752, 823, 859, 926, 969, 996, 1027, 1052, 1071, 1111, 1155, 1199, 1265, 1299, 1326, 1371, 1474, 1562, 2904, 3158 cm^{-1}; elemental analysis calcd (%) for $C_7H_{18}ClN_3O_6$ (275.69): C 30.50, H 6.58, N 15.24; found: C 30.45, H 5.73, N 15.24.

The free amine **P3**$\cdot 0.5H_2O$ was obtained in quantitative yield as a white solid by ion-exchange chromatography on Dowex 2-X8 (OH^- form). ^1H NMR (D_2O, pH*=11):[43] $\delta=3.38$ (t, $J=6$ Hz, 1H), 3.61 (m′, 2H), 3.78 (dd, $J_1=6$, $J_2=2$ Hz, 2H), 3.88 ppm (m, 1H); ^{13}C NMR (D_2O, pH*>12):[43] $\delta=55.1$, 58.4, 62.1, 71.7, 160.1 ppm; IR: $\tilde{\nu}=607$, 691, 759, 825, 856, 976, 995, 1038, 1053, 1075, 1167, 1188, 1227, 1282, 1328, 1401, 1505, 1642, 3264, 3322 cm^{-1}; elemental analysis calcd (%) for $C_7H_{14}N_3O_{4.5}$ (212.20): C 39.62, H 6.65, N 19.80; found: C 40.37, H 6.65, N 19.82.

7,7′-(Ethane-1,2-diylbis(azanediyl))bis(6,8,9-trihydroxy-2,4-diazabicyclo-[3.3.1]nonan-3-one) (P4): The amine **P3**$\cdot 0.5H_2O$ (1.0 g, 4.71 mmol) was suspended in H_2O (10 mL), and an aqueous 40% solution of glyoxal (290 μL, 357 mg, 2.46 mmol) was added. The resulting suspension was stirred at room temperature. A slow color change to yellow was observed. After 24 h, the unreacted **P3** was filtered off (this material may be regenerated and used in a further experiment, see below). $NaBH_4$ (from Alfa Aesar GmbH, ≈97% purity; 1 g, ≈25 mmol) was then slowly added in small portions to the yellow solution. The mixture was stirred for 2 h. The solution was then acidified to pH 1 with 1 M aqueous HCl and evaporated to dryness under reduced pressure. The residue was dissolved in a few mL of an aqueous 0.5 M HCl solution and sorbed on Dowex 50W-X2. The column was successively eluted with H_2O (0.5 L), aqueous 0.5 M HCl (1.0 L) and aqueous 3 M HCl (1.0 L). The last fraction was evaporated to dryness and dried in vacuo for 24 h. The product was isolated as a white, hydrated trihydrochloride **P4**$\cdot 3HCl\cdot 5H_2O$ (1.01 g, 1.60 mmol, 68%). ^1H NMR (D_2O, pH*<2):[43] $\delta=3.59$ (s, 4H), 3.74 (t,

$J=2$ Hz, 4H), 3.93 (t, $J=2$ Hz, 2H), 3.96 (t, $J=6$ Hz, 2H), 4.21 ppm (dd, $J_1=6$, $J_2=2$ Hz, 4H); ^{13}C NMR (D_2O, pH*<2):[43] $\delta=48.6$, 57.9, 61.3, 62.3, 69.0, 159.6 ppm; IR: $\tilde{\nu}=583$, 884, 909, 1053, 1177, 1393, 1506, 1644, 3192 cm^{-1}; elemental analysis calcd (%) for $C_{16}H_{41}Cl_3N_6O_{13}$ (631.89): C 30.41, H 6.54, N 13.30; found: C 30.38, H 6.56, N 13.69.

Regeneration of the unreacted P3: The filtered solid was dissolved in a minimal amount of H_2O and acidified to a pH of 1 with aqueous HCl. This solution was sorbed on Dowex 50W-X2, and the column was eluted with H_2O, 0.2 M aqueous HCl and 0.5 M aqueous HCl. The last fraction was evaporated to dryness and dried in vacuo. This product could be used as starting material for the synthesis of additional **P4**·3HCl·5H_2O without further purification.

The free amine **P4**·3H_2O was obtained in quantitative yield (white solid) by ion-exchange chromatography on Dowex 2-X8 (OH^- form). ^{1}H NMR (D_2O, pH*> 12):[43] $\delta=2.71$ (s, 4H), 3.12 (t, $J=6$ Hz, 2H), 3.58 (m′, 4H), 3.81 (dd, $J_1=6$, $J_2=2$ Hz, 4H), 3.85 ppm (t, $J=2$ Hz, 2H); ^{13}C NMR (D_2O, pH*> 12):[43] $\delta=54.6$, 58.4, 62.1, 62.4, 71.8, 159.8 ppm; IR: $\tilde{\nu}=$ 873, 1044, 1219, 1338, 1397, 1508, 1636, 1716, 2858, 3246, 3735 cm^{-1}; elemental analysis calcd (%) for $C_{16}H_{34}N_6O_{11}$ (486.47): C 39.50, H 7.04, N 17.28; found: C 40.04, H 6.97, N 17.34.

***all-cis*-N^1,N^2-Bis(2,4,6-trihydroxy-3,5-diaminocyclohexyl)ethane-1,2-diamine (L^e)**: The solid bis-urea-amine **P4**·3H_2O (0.40 g, 0.82 mmol) and solid NaOH (4.0 g, 0.10 mol) were dissolved in an ethyleneglycol/H_2O mixture (3:1) and heated to 125 °C (temperature of the reaction mixture) for 24 h. A color change from light yellow to dark brown was observed. The reaction mixture was then allowed to cool to room temperature. It was acidified to a pH 1 with 1 M aqueous HCl. Some precipitation occurred around pH 7, but the precipitate redissolved by addition of the remaining acid. The resulting clear, yellow solution was sorbed on Dowex 50W-X2, and the column was successively eluted with H_2O (1 L), aqueous 1 M and 3 M HCl (each 1 L) and aqueous 6 M HCl (2 L). The last fraction was evaporated under reduced pressure to a total volume of about 100 mL. A yellowish solid precipitated. It was filtered off and dried in vacuo for 24 h. This product (0.414 g, 0.64 mmol, 78%) was characterized as L^e·6HCl·2.5H_2O. ^{1}H NMR (D_2O, pH*<2):[43] $\delta=3.75$ (t, $J=3$ Hz, 4H), 3.79 (s, 4H), 3.88 (t, $J=3$ Hz, 2H), 4.47 (t, $J=3$ Hz, 2H), 4.61 ppm (t, $J=3$ Hz, 4H); ^{13}C NMR (D_2O, pH*<2):[43] $\delta=43.6$, 53.3, 60.5, 67.3, 68.7 ppm; IR: $\tilde{\nu}=568$, 645, 763, 848, 896, 948, 1037, 1114, 1139, 1285, 1361, 1422, 1480, 1568, 2838 cm^{-1}; elemental analysis calcd (%) for $C_{14}H_{43}Cl_6N_6O_{8.5}$ (644.24): C 26.10, H 6.73, N 13.04; found: C 26.09, H 6.67, N 12.79.

Regeneration of unreacted P4: The 3 M HCl fraction of the abovementioned cation-exchange chromatography was evaporated under reduced pressure to a total volume of a few mL. Addition of MeOH (20 mL) resulted in the precipitation of a white solid that was filtered off and dried in vacuo. It could be used as starting material for the synthesis of additional L^e·6HCl·2.5H_2O without further purification.

The free amine L^e·6H_2O was obtained quantitatively as a white solid by ion-exchange chromatography on Dowex 2-X8 (OH^- form). ^{1}H NMR (D_2O, 1 M KOD): $\delta=2.60$ (t, $J=2.5$ Hz, 2H), 2.68 (t, $J=2.5$ Hz, 4H), 2.84 (s, 4H), 3.84 (m′, 2H), 4.03 ppm (m′, 4H); ^{13}C NMR (D_2O, 1 M KOD): $\delta=47.5$, 55.8, 61.5, 76.3, 79.9 ppm; IR: $\tilde{\nu}=770$, 798, 888, 916, 951, 996, 1074, 1091, 1127, 1166, 1250, 1353, 1446, 1571, 1669, 2699, 2894, 3071, 3344, 3447 cm^{-1}; elemental analysis calcd (%) for $C_{14}H_{44}N_6O_{12}$ (488.53): C 34.42, H 9.08, N 17.20; found: C 34.32, H 8.25, N 17.22.

[$Na_{0.5}$(H_6L^e)]($BiCl_6$)$_2$$Cl_{0.5}$·4$H_2O$ (1): L^e·6HCl·2.5H_2O (40 mg, 62 μmol) was dissolved in 3 M aqueous HCl (1 mL). NaCl (4 mg, 68 μmol) and Bi(NO_3)$_3$·5H_2O (60 mg, 124 μmol) were added. The solution was kept at 0 °C for several days to give colorless needles that were suitable for single crystal X-ray analysis. The Na/Bi ratio of this compound determined by ICP-OES was 3.83 ± 0.08.

[Ni(L^e)]Cl_2·5H_2O (2): L^e·6H_2O (41 mg, 84 μmol) was dissolved in H_2O (1 mL). Solid $NiCl_2$·6H_2O (20 mg, 84 μmol) was added. Slow evaporation of the solvent at ambient temperature yielded pink crystals that could be used for a single-crystal X-ray analysis. The dried product analyzed for [Ni(L^e)]Cl_2·H_2O. IR: $\tilde{\nu}=551$, 559, 580, 744, 772, 829, 857, 904, 1004, 1049, 1122, 1166, 1225, 1267, 1326, 1359, 1569, 2358, 2897, 3193, 3355 cm^{-1}; UV/Vis (H_2O): $\lambda_{max}=321$, 511, 799 nm; elemental analysis calcd (%) for $C_{14}H_{34}Cl_2N_6NiO_7$ (528.06): C 31.84, H 6.49, N 15.92; found: C 32.41, H 6.59, N 15.81.

[Cu(L^e)](ClO_4)$_2$·H_2O (3):[22] L^e·6H_2O (40 mg, 82 μmol) was dissolved in H_2O (1 mL). Solid $Cu(ClO_4)_2$·6H_2O (30 mg, 81 μmol) was added. Slow evaporation of the solvent at ambient temperature yielded crystals that could be used for single-crystal X-ray analysis. IR: $\tilde{\nu}=597$, 620, 750, 784, 823, 858, 885, 904, 928, 1037, 1210, 1236, 1289, 1348, 1392, 1458, 1567, 2359, 2886, 3238, 3271, 3316, 3348 cm^{-1}; UV/Vis (H_2O): $\lambda_{max}=603$ nm; elemental analysis calcd (%) for $C_{14}H_{34}Cl_2CuN_6O_{15}$ (660.90): C 25.44, H 5.19, N 12.72; found: C 25.89, H 5.05, N 12.50.

[Zn(L^e)]CO_3·7H_2O (4): L^e·6H_2O (40 mg, 82 μmol) was dissolved in H_2O (1 mL). Solid $Zn(NO_3)_2$·6H_2O (24 mg, 81 μmol) was added. The solution was exposed to air, thus allowing the uptake of atmospheric CO_2. Slow evaporation of the solvent resulted in the formation of a small amount of colorless crystals that could be used for single-crystal X-ray analysis.

[Co(L^e)]Cl_3·5H_2O (5a): L^e·6HCl·2.5H_2O (0.46 g, 715 μmol) was dissolved in H_2O (60 mL). The pH of the solution was adjusted to 8.5 by adding 0.1 M NaOH. Solid $CoCl_2$·6H_2O (170 mg, 715 μmol) was added, resulting in a red-orange solution that was aerated with a steady stream of air for 24 h. The solution was sorbed onto Dowex 50W-X2, and the column was successively eluted with H_2O (150 mL), aqueous 0.5 M HCl (150 mL), aqueous 1 M HCl (150 mL) and aqueous 3 M HCl (150 mL). The last fraction was evaporated to dryness, and the resulting orange solid was dried in vacuo (orange powder, 359 mg, 565 μmol, 79%). ^{1}H NMR (D_2O, pH*=3.80):[43] $\delta=2.81$ (m′, 2H), 2.94 (m′, 2H), 3.03 (m′, 2H), 3.24 (d, $J=8$ Hz, 2H), 3.98 (d, $J=8$ Hz, 2H), 4.09 (m′, 2H), 4.166 (m′, 2H) 4.174 ppm (m′, 2H); ^{13}C NMR (D_2O, pH*=3.80):[43] $\delta=52.5$ (2 C), 56.5, 61.1, 65.4, 67.0, 67.5 ppm;[30] IR: $\tilde{\nu}=553$, 803, 861, 930, 1062, 1238, 1339, 1557, 3120; UV/Vis (H_2O): λ_{max} (ε)=340 (94), 471 nm (87 M^{-1}cm^{-1}); elemental analysis calcd (%) for $C_{14}H_{42}Cl_3CoN_6O_{11}$ (635.81): C 26.45, H 6.66, N 13.22; found: C 26.57, H 6.41, N 13.13.

[Co(L^e)][$ZnCl_4$]Cl (5b): A sample of **5a** (50 mg, 79 μmol) was dissolved in H_2O. Solid $ZnCl_2$ (11 mg, 81 μmol) was added, and the solution was acidified to pH <1 with 3 M aqueous HCl. Orange crystals appeared after slow evaporation of the solvent.[21]

[Co(L^e)](ClO_4)$_3$ (5c):[22] A sample of **5a** (20 mg, 31 μmol) was dissolved in 0.5 mL of aqueous 17.5% $HClO_4$. Slow evaporation of the solvent at ambient temperature over a period of two weeks gave orange crystals (80%) suitable for single-crystal X-ray analysis.

[Ga(H_{-2}L^e)]NO_3·2H_2O (6): Single crystals of **6** that were suitable for X-ray analysis were obtained following the protocol of the Cu complex **3**, using solid, hydrous Ga(NO_3)$_3$ and L^e·6H_2O as starting materials.

Cyclic voltammetry: Scans were recorded at ambient temperature (25±2 °C) in a BAS C2 cell by using a BAS 100B/W2 potentiostat, a Au (Mn complex) or a Pt (Co and Ni complex) working electrode, a Pt counter electrode and a Ag/AgCl reference electrode. 0.1 M KCl was used as supporting electrolyte. Samples of the Co and Ni complexes were prepared by dissolving solid [Co(L^e)]Cl_3·5H_2O (**5a**) or [Ni(L^e)]Cl_2·5H_2O (**2**) in H_2O, respectively, and by adjusting the pH to 9 using 0.1 M KOH. Samples of the Mn complex were prepared in situ using $MnCl_2$ and L^e·6HCl·2.5H_2O. 0.5 M KOH was then added to adjust the pH to a value of 12. The metal concentration of all samples was 1 mM.

Molecular mechanics calculations: Considering the four different binding sites shown in Scheme 1, a total of 10 combinations must be considered for the two subunits in a metal complex ML^e. This number increases to more than 200, if additional *cis–trans* diastereomers, as well as the various possible linking interactions, are taken into account. However, owing to the relatively short tether length of the ethylene bridge, some of these structures are obviously not meaningful. A total of 15 relevant isomers were finally selected for the calculations. Some of them could exist in a zwitterionic or non-zwitterionic form (Scheme 1b), and both forms were considered when appropriate. In addition, different conformations of the ethylene bridge were taken into account for some of the structures. A first draft of each structure was generated using the program Hyperchem.[44] The energy minimization was performed using the program Momec97[45] with an extension of the force field as described in reference [9]. All metal complexes were modeled with Co^{III}. A validation of

this force field for such complexes is found in reference [46]. In a first step, geometry optimization was performed with the full-matrix Newton–Raphson algorithm. To avoid location of false (local) minima, a search for further low-energy conformers was performed using the "Random Kick" option of Momec97. In many cases this procedure did not reveal any conformation of lower energy. However, in a few cases structures of considerably lower energy were found and those were once more energy minimized. The calculated structures generally exhibited bond distances and bond angles as expected, with the exception of some Co–O and Co–N bond lengths in oxygen-rich coordination spheres (CoO_xN_{6-x}, $x \geq 3$) that seem to be slightly underestimated (1.92–1.94 Å). All energy minimization calculations reached convergence (<0.005 Å). A detailed presentation of the results of these calculations is given in Table S1 in the Supporting Information.

NMR titration: A solution of $L^e \cdot 6HCl \cdot 2.5H_2O$ (total $L^e = 26$ mM) and KCl (0.1 M) in D_2O (30 mL) was neutralized stepwise by adding small increments of a NaOD/D_2O solution (0.1 M). After each addition of base, the pH* was measured,[43] and a 0.6 mL aliquot was taken for the recording of a ^1H NMR spectrum. A total of 41 spectra were recorded. Least squares calculations $\Sigma(\delta_{obs}-\delta_{calcd})^2 = \min$ were performed assuming a rapid equilibrium between the differently protonated species $H_x(L^e)^{x+}$ ($0 \leq x \leq 6$), using the computer program NMR-Tit.[47] The calculations revealed an excellent fit (Figure 2) with meaningful and robust values for pK_{a1} (3.23) and pK_{a6} (9.02). However, the calculations also showed that the intermediate values could vary over a wide range without a significant influence on the accuracy of the fit. In contrast to the potentiometric measurements (see next section), the high number of species, that all coexist in significant proportions around $5 < pH < 8$, did not allow an unambiguous determination of the intermediate pK_{ax} values ($2 \leq x \leq 5$) by this method.

Potentiometric and spectrophotometric titrations: Titration experiments were performed at 25.0 °C under N_2 (scrubbed with an aqueous solution of the pure inert electrolyte) as described previously.[48] For the determination of the pK_a values of $H_6(L^e)^{6+}$, several alkalimetric titrations were carried out with analytically pure samples of $L^e \cdot 6HCl \cdot 2.5H_2O$ (total $L^e = 1.0$ mM), using KCl (0.1 or 1.0 M) or KNO_3 (1.0 M) as inert electrolyte. The formation constants of metal complexes were determined using solutions that contained $L^e \cdot 6HCl \cdot 2.5H_2O$ and the metal salt in 2:1, 1:1 or 1:2 molar ratios (total L^e and total M varied between 0.5 and 2 mM) at an ionic strength of 0.1 M (KCl). In the case of Cu^{II}, titrations with an equimolar ratio were also performed in 1 M KCl and 1 M KNO_3 with a total metal and a total ligand concentration of 10 mM. Standardized stock solutions of $L^e \cdot 6HCl \cdot 2.5H_2O$ and of the corresponding metal salts were used for sample preparations. Complete equilibration was ensured by back titrations for all metal-containing solutions. A Metrohm piston burette was used for the addition of the titrant (KOH, HCl or HNO_3), and the pH was recorded using a Metrohm glass electrode with an incorporated Ag/AgCl reference connected to a Metrohm 713 pH meter. The stability of the electrode was checked by a calibration titration prior to and after each measurement. For spectrophotometric measurements, the titration cell was equipped with an immersion probe (HELLMA), that was connected to a spectrophotometer equipped with a diode array detector (J&M, TIDAS-UV/NIR/100–1). A PC was used to trigger the recording of a spectrum just prior to the addition of each new aliquot of base.[48]

Calculations of equilibrium constants: Equilibrium constants were generally calculated as concentration quotients ($pH = -\log[H^+]$) by using the computer programs Hyperquad2000 and Specfit.[49,50] The total concentrations of the reactants and the pK_w (13.78 for $\mu = 0.1$ M, 13.77 for $\mu = 1.0$ M) were not refined.[37] The protonation constants of the ligand L^e were evaluated separately and were kept fixed when refining formation constants of the metal-containing species. The UV/Vis spectrum of the free Cu^{2+} was recorded separately and was imported as a fixed data set for the evaluation of the formation constants of the Cu complexes. The free ligand and its protonation products were treated as nonabsorbing species. The stability of Cu^{II}-chloro complexes of composition $[Cu_x(L^e)_yH_zCl_q]^{2x+z-q}$ was calculated from the titration experiments performed in 1.0 M KCl. The formation constants of these species were refined, whereas the formation constants of the corresponding Cl-free $[Cu_x(L^e)_yH_z]^{2x+z}$ species, that were determined in a 1.0 M KNO_3 medium were considered as fixed values. The evaluated value of 0.58(2) for $\log \beta_{CuCl}$ is in reasonable agreement with the literature[51] and thus supports the reliability of this method.

Single-crystal X-ray diffraction studies: Data sets were collected by using the following diffractometers: Bruker X8-APEX (**1**, **2**, **6**), STOE Stadi4 (**3**, **4**), and Bruker Smart (**5c**). Graphite-monochromated $Mo_{K\alpha}$ radiation ($\lambda = 0.71073$ Å) was used in all experiments. The data were collected at 90(2) K (**5c**), 100(2) K (**1**, **2**, **6**) or ambient temperature (**3**, **4**). Further details of data collection and structure solutions are summarized in Tables 4 and 5. The structures were solved by direct methods (SHELXS-97) and refined by full-matrix, least-squares calculations on F^2 (SHELXL-97).[52] Disorder: Na1 and Cl11 of **1** were refined with site occupancies of 50%. It was further noted that the anisotropic displacement ellipsoid of Cl11, which is placed on a mirror plane, deviates significantly from a spherical shape. Attempts were made to resolve this disorder in terms of a superstructure considering the space groups $P2_1/m$, $Pmc2_1$ or $Pmn2_1$, but were not successful.[53] One of the oxygen atoms of a ClO_4^- counter ion of **3** was distributed over two positions having a site occupancy of 50%. One of the ClO_4^- counter ions of **5c** was located in proximity of a two fold rotational axis and was refined in terms of a superposition of two half occupied moieties (Cl1, O8, O9), having the fully occupied O10 and O10A in common. In addition, the ethylene bridge (C1, C2 and

Table 4. Crystallographic data for $[Na_{0.5}(H_6L^e)](BiCl_6)_2Cl_{0.5} \cdot 4H_2O$ (**1**), $[Ni(L^e)]Cl_2 \cdot 5H_2O$ (**2**), and $[Cu(L^e)](ClO_4)_2 \cdot H_2O$ (**3**).

	1	**2**	**3**
chemical formula	$C_{14}H_{46}Bi_2Cl_{12.5}N_6Na_{0.5}O_{10}$	$C_{14}H_{42}Cl_2N_6NiO_{11}$	$C_{14}H_{34}Cl_2CuN_6O_{15}$
formula weight	1331.15	600.15	660.91
space group	*Pnma* (No. 62)	$P2_1/c$ (No. 14)	$P2_1/c$ (No. 14)
crystal system	orthorhombic	monoclinic	monoclinic
a [Å]	14.7530(10)	13.086(3)	19.500(4)
b [Å]	12.5057(9)	13.259(3)	9.171(2)
c [Å]	21.2619(15)	14.374(3)	14.430(3)
α [°]	90.00	90.00	90.00
β [°]	90.00	96.98(3)	107.58(3)
γ [°]	90.00	90.00	90.00
V [Å^3]	3922.7(5)	2475.7(9)	2460.1(9)
dimensions [mm]	$0.55 \times 0.21 \times 0.12$	$0.30 \times 0.25 \times 0.20$	$0.30 \times 0.20 \times 0.20$
ρ_{calcd} [g cm^{-3}]	2.254	1.610	1.784
μ [cm^{-1}]	9.867	1.064	1.191
Z	4	4	4
T [K]	100(2)	100(2)	293(2)
max., min. transmission	0.3839, 0.0741	0.8153, 0.7407	[a]
$2\theta_{max}$	50.00	52.00	48.00
data, parameters	3624, 293	4864, 411	3801, 407
R_1 [$I > 2\sigma(I)$][b]	0.0161	0.0261	0.0422
wR_2 (all data)[c]	0.0424	0.0690	0.1138
max/min res. e-density, [eÅ^{-3}]	1.157/−0.680	1.050/−0.535	0.673/−0.540

[a] An absorption correction was not performed. [b] $R_1 = \Sigma||F_o| - |F_c||/\Sigma|F_o|$. [c] $wR_2 = [\Sigma w(F_o^2 - F_c^2)^2/\Sigma wF_o^4]^{1/2}$.

Table 5. Crystallographic data for $[Zn(L^e)]CO_3{\cdot}7H_2O$ (**4**), $[Co(L^e)](ClO_4)_3$ (**5c**), and $[Ga(H_{-2}L^e)]NO_3{\cdot}2H_2O$ (**6**).

	4	**5c**	**6**
chemical formula	$C_{15}H_{46}N_6O_{16}Zn$	$C_{14}H_{32}Cl_3CoN_6O_{18}$	$C_{14}H_{34}GaN_7O_{11}$
formula weight	631.95	737.74	546.20
space group	*Pbcn* (No. 60)	*C*2/*c* (No. 15)	Cc (No. 9)
crystal system	orthorhombic	monoclinic	monoclinic
a [Å]	13.542(3)	16.2096(9)	13.887(3)
b [Å]	14.476(3)	11.0975(6)	12.340(3)
c [Å]	26.680(5)	14.6272(8)	13.755(3)
α [°]	90.00	90.00	90.00
β [°]	90.00	104.3480(10)	112.61(3)
γ [°]	90.00	90.00	90.00
V [Å]^3	5230.2(19)	2549.2(2)	2176.2(8)
dimensions [mm]	0.30×0.15×0.10	0.40×0.30×0.20	0.40×0.30×0.20
ρ_{calcd} [g cm^{-3}]	1.605	1.922	1.667
μ [cm^{-1}]	1.025	1.087	1.338
Z	8	4	4
T [K]	293(2)	90(2)	100(2)
max., min. transmission	[a]	0.8120, 0.6703	0.7758, 0.6167
$2\theta_{max}$	47.0	56.54	48.02
data, parameters	3865, 395	3164, 217	3202, 376
R_1 [$I > 2\sigma(I)$][b]	0.0785	0.0784	0.0355
wR_2 (all data)[c]	0.2272	0.1850	0.0924
max/min res. e-density [eÅ^{-3}]	0.933/−0.766	0.858/−1.192	0.668/−0.260

[a] An absorption correction was not performed. [b] $R_1 = \Sigma||F_o| - |F_c||/\Sigma|F_o|$. [c] $wR_2 = [\Sigma w(F_o^2 - F_c^2)^2/\Sigma wF_o^4]^{1/2}$.

the corresponding hydrogen atoms) of the L^e-ligand that is duplicated by an inversion center was also refined with a 50% occupancy. Inspection of interatomic distances clearly indicated that the two disorder problems are dependent on each other. Two oxygen atoms (O1, O3) of the NO_3^- counter ion of **6** were found to be equally distributed over two sites. These were considered with 50% site occupancies. Anisotropic displacement parameters were refined for all non-hydrogen atoms. All O–H and N–H hydrogen atoms of **1**, **2** and **3** were located and refined with variable isotropic displacement parameters. The OH hydrogen atoms of **4** were located and refined with isotropic displacement parameters fixed at $1.5\,U_{eq}$ of the parent oxygen atoms; however, only one hydrogen atom could be located for the water oxygen atom O400. For **6**, the O–H and N–H hydrogen atoms were also located and refined with a variable U_{iso}, except the N–H hydrogen atoms H3NA and H3NB that were refined with U_{iso} fixed at $1.2\,U_{eq}$ of N31. All other hydrogen atomic positions were calculated (riding model). CCDC-747720 (**5b**), CCDC-747721 (**5c**), CCDC-747722 (**3**), CCDC-747723 (**6**), CCDC-747724 (**1**), CCDC-747725 (**2**), and CCDC-747726 (**4**) contain the supplementary crystallographic data for this paper. These data can be obtained free of charge from The Cambridge Crystallographic Data Centre via www.ccdc.cam.ac.uk/data_request/cif.

Acknowledgements

We thank Dr. Volker Huch (Universität des Saarlandes) for the acquisition of the X-ray data and Dr. Thomas Weyhermüller (Max-Planck-Institut für Bioanorganische Chemie, Mühlheim), Dr. Holger Kohlmann (Universität des Saarlandes), and Prof. Jon Zubieta (Syracuse University) for help and advice.

[1] a) K. F. Sibbons, K. Shastri, M. Watkinson, *Dalton Trans.* **2006**, 645–661; b) R. Hage, A. Lienke, *J. Mol. Catal. A-Chem* **2006**, *251*, 150–158.

[2] a) B. R. Bodsgard, R. W. Clark, A. W. Ehrbar, J. N. Burstyn, *Dalton Trans.* **2009**, 2365–2373; b) M. Scarpellini, J. Gätjens, O. J. Martin, J. W. Kampf, S. E. Sherman, V. L. Pecoraro, *Inorg. Chem.* **2008**, *47*, 3584–3593; c) J. W. de Boer, W. R. Browne, J. Brinksma, P. L. Alsters, R. Hage, B. L. Feringa, *Inorg. Chem.* **2007**, *46*, 6353–6372; d) V. B. Romakh, B. Therrien, G. Süss-Fink, G. B. Shul′pin, *Inorg. Chem.* **2007**, *46*, 3166–3175; e) F. H. Fry, A. J. Fischmann, M. J. Belousoff, L. Spiccia, J. Brügger, *Inorg. Chem.* **2005**, *44*, 941–950; f) Q.-X. Li, Q.-H. Luo, Y.-Z. Li, M.-C. Shen, *Dalton Trans.* **2004**, 2329–2335.

[3] a) Y. Kajita, H. Arii, T. Saito, Y. Saito, S. Nagatomo, T. Kitagawa, Y. Funahashi, T. Ozawa, H. Masuda, *Inorg. Chem.* **2007**, *46*, 3322–3335; b) A. K. Nairn, S. J. Archibald, R. Bhalla, B. C. Gilbert, E. J. MacLean, S. J. Teat, P. H. Walton, *Dalton Trans.* **2006**, 172–176; c) E. A. Lewis, H. H. Khodr, R. C. Hider, J. R. Lindsay Smith, P. H. Walton, *Dalton Trans.* **2004**, 187–188.

[4] a) K. Wieghardt, I. Tolksdorf, W. Herrmann, *Inorg. Chem.* **1985**, *24*, 1230–1235; b) D. Hanke, K. Wieghardt, B. Nuber, R.-S. Lu, R. K. McMullan, T. F. Koetzle, R. Bau, *Inorg. Chem.* **1993**, *32*, 4300–4305; c) R. Haidar, M. Ipek, B. DasGupta, M. Yousaf, L. J. Zompa, *Inorg. Chem.* **1997**, *36*, 3125–3132.

[5] D. Parker, K. Senanayake, J. Vepsailainen, S. Williams, A. S. Batsanov, J. A. K. Howard, *J. Chem. Soc. Perkin Trans. 2* **1997**, 1445–1452.

[6] H. Egli, PhD Thesis, ETH Zürich (Zürich), **1975**.

[7] F. Mancin, E. Rampazzo, P. Tecilla, U. Tonellato, *Eur. J. Org. Chem.* **2004**, 281–288.

[8] K. Hegetschweiler, *Chem. Soc. Rev.* **1999**, *28*, 239–249.

[9] D. Kuppert, P. Comba, K. Hegetschweiler, *Eur. J. Inorg. Chem.* **2006**, 2792–2807.

[10] M. Weber, B. Morgenstern, K. Hegetschweiler, H. W. Schmalle, *Helv. Chim. Acta* **2001**, *84*, 571–578.

[11] Rotation around the N–C and C–C bonds of the diaminoethane bridge of $H_6(L^e)^{6+}$ generates a series of conformers with a C_2- and a C_i-symmetric rotamer being of lowest energy (see Chart S1 in the Supporting Information). These two conformers have either two homotopic or two enantiotopic cyclohexane rings with six different carbon atoms per ring. The C_i-symmetric conformer was observed in the crystal structure of the sodium complex (see Figure 3). Additional conformers with C_{2h} or C_{2v} symmetry, having either a *transoid* or *cisoid* arrangement of the N-C-C-N fragment, are of slightly higher energy. Due to rapid interconversion of all these rotamers within the NMR time scale, an averaged structure with two homotopic cyclohexane rings was observed. Within each ring, four of the six carbon atoms (C2, C2′; C3, C3′) belong to two constitutionally heterotopic pairs of enantiotopic CH groups. Thus, the two cyclohexane residues exhibit four resonances in the ^{13}C and in the ^1H NMR spectra. The ethylene bridge leads to one additional resonance in both spectra. For the terminology of topicity, see: a) H. Hirschmann, K. R. Hanson, *Eur. J. Biochem.* **1971**, *22*, 301–309; b) K. Mislow, *Bull. Soc. Chim. Belg.* **1977**, *86*, 595–601. A comprehensive discussion of the symmetry properties of such non-rigid molecules can be found in: c) H. C. Longuet-Higgins, *Mol. Phys.* **1963**, *6*, 445–460; d) H. C. Longuet-Higgins, *Mol. Phys.* **2002**, *100*, 11–20.

[12] a) A. Bianchi, M. Micheloni, P. Paoletti, *Coord. Chem. Rev.* **1991**, *110*, 17–113; b) S. Kubik, C. Reyheller, S. Stüwe, *J. Inclusion Phenom. Macrocyclic Chem.* **2005**, *52*, 137–187.

[13] M. Weber, D. Kuppert, K. Hegetschweiler, V. Gramlich, *Inorg. Chem.* **1999**, *38*, 859–868.
[14] a) D. Kuppert, J. Sander, C. Roth, M. Wörle, T. Weyhermüller, G. J. Reiss, U. Schilde, I. Müller, K. Hegetschweiler, *Eur. J. Inorg. Chem.* **2001**, 2525–2542; b) K. Hegetschweiler, O. Maas, A. Zimmer, R. J. Geue, A. M. Sargeson, J. Harmer, A. Schweiger, I. Buder, G. Schwitzgebel, V. Reiland, W. Frank, *Eur. J. Inorg. Chem.* **2003**, 1340–1354.
[15] J. W. Pauly, J. Sander, D. Kuppert, M. Winter, G. J. Reiss, F. Zürcher, R. Hoffmann, T. F. Fässler, K. Hegetschweiler, *Chem. Eur. J.* **2000**, *6*, 2830–2846.
[16] J. Romba, D. Kuppert, B. Morgenstern, C. Neis, S. Steinhauser, T. Weyhermüller, K. Hegetschweiler, *Eur. J. Inorg. Chem.* **2006**, 314–328.
[17] a) K. Hegetschweiler, M. Wörle, M. D. Meienberger, R. Nesper, H. W. Schmalle, R. D. Hancock, *Inorg. Chim. Acta* **1996**, *250*, 35–47; b) K. Hegetschweiler, A. Egli, E. Herdtweck, W. A. Herrmann, R. Alberto, V. Gramlich, *Helv. Chim. Acta* **2005**, *88*, 426–434; c) A. Kramer, R. Alberto, A. Egli, I. Novak-Hofer, K. Hegetschweiler, U. Abram, P. V. Bernhardt, P. A. Schubiger, *Bioconjugate Chem.* **1998**, *9*, 691–702.
[18] The sum of the ionic radii of a hexacoordinate Na^{I} and a tricoordinate O^{-II} is 2.38 Å; see: a) R. D. Shannon, *Acta Crytallogr. Sect. A* **1976**, *32*, 751–767. Na–O bond lengths of related structures, where a hexacoordinate Na^{I} cation is bonded to alcoholic oxygen atoms range from 2.29–2.47 Å: b) F. A. Cotton, M. P. Diebold, W. J. Roth, *Inorg. Chem.* **1988**, *27*, 3596–3600; c) D. Szeymies, B. Krebs, G. Henkel, *Angew. Chem.* **1984**, *96*, 797–798; *Angew. Chem. Int. Ed. Engl.* **1984**, *23*, 804–805; d) M. Capo, J. M. Saa, A. Alvarez, *Chem. Commun.* **2002**, 1982–1983; e) D. E. Berning, K. V. Katti, C. L. Barnes, W. A. Volkert, *Chem. Ber./Recueil* **1997**, *130*, 907–911.
[19] D. Cremer, J. A. Pople, *J. Am. Chem. Soc.* **1975**, *97*, 1354–1358.
[20] The disorder can be explained in terms of a superposition of the *lel* and *ob* isomer; a view of the $[Co(L^{e})]^{3+}$ ion is shown in Figure S1 in the Supporting Information.
[21] $C_{14}H_{32}Cl_5CoN_6O_6Zn$, monoclinic, space group $P2_1/m$, $a=9.219(3)$ Å, $b=13.876(5)$ Å, $c=10.517(3)$ Å, $\beta=99.054(16)°$, $Z=2$, $T=100(2)$ K, 2377 unique reflections, 203 refined parameters, $R_1=0.105$, wR_2 (all data) $=0.313$.
[22] **Caution!** Perchlorate salts of metal complexes with organic ligands are potentially explosive.
[23] M. Ghisletta, H.-P. Jalett, T. Gerfin, V. Gramlich, K. Hegetschweiler, *Helv. Chim. Acta* **1992**, *75*, 2233–2242.
[24] K. Hegetschweiler, V. Gramlich, M. Ghisletta, H. Samaras, *Inorg. Chem.* **1992**, *31*, 2341–2346.
[25] G. J. Reiss, W. Frank, K. Hegetschweiler, D. Kuppert, *Acta Crystallogr. Sect. C* **1998**, *54*, 614–616.
[26] a) E. I. Stiefel, G. F. Brown, *Inorg. Chem.* **1972**, *11*, 434–436; b) A. Avdeef, J. P. Fackler, *Inorg. Chem.* **1975**, *14*, 2002–2006.
[27] P. Comba, A. M. Sargeson, L. M. Engelhardt, J. M. Harrowfield, A. H. White, E. Horn, M. R. Snow, *Inorg. Chem.* **1985**, *24*, 2325–2327.
[28] A. G. Orpen, L. Brammer, F. H. Allen, O. Kennard, D. G. Watson, R. Taylor, *J. Chem. Soc. Dalton Trans.* **1989**, S1–S83.
[29] M. Melník, M. Kabesova, L. Macaskova, C. E. Holloway, *J. Coord. Chem.* **1998**, *45*, 31–145.
[30] The two types of diastereotopic carbon atoms, carrying a primary amino group, exhibited an identical chemical shift of $\delta=52.5$ ppm.
[31] K. Hegetschweiler, M. Ghisletta, T. F. Fässler, R. Nesper, H. W. Schmalle, G. Rihs, *Inorg. Chem.* **1993**, *32*, 2032–2041.
[32] A. Zimmer, D. Kuppert, T. Weyhermüller, I. Müller, K. Hegetschweiler, *Chem. Eur. J.* **2001**, *7*, 917–931.
[33] M. DeRonde, D. Driscoll, R. Yang, L. J. Zompa, *Inorg. Nucl. Chem. Lett.* **1975**, *11*, 521–523.
[34] E. Prenesti, P. G. Daniele, M. Prencipe, G. Ostacoli, *Polyhedron* **1999**, *18*, 3233–3241.
[35] J. Bjerrum, B. V. Agarwala, *Acta Chem. Scand. A* **1980**, *34*, 475–481.
[36] For 1,5,9,12,16,20-hexaazaicosane, the formation constant for the dinuclear species $[Cu_2L]^{4+}$ is $\log\beta_{210}=27.12$ (25 °C, $\mu=0.15$ M, from Ref. [37]). This value has to be compared with 26.09, observed for L^{e} (Table 2).
[37] Critically Selected Stability Constants of Metal Complexes, NIST Standard Reference Database 46, Version 8.0, R. M. Smith, A. E. Martell, R. J. Motekaitis, Gaithersburg, **2004**.
[38] M. Ghisletta, L. Hausherr-Primo, K. Gajda-Schrantz, G. Machula, L. Nagy, H. W. Schmalle, G. Rihs, F. Endres, K. Hegetschweiler, *Inorg. Chem.* **1998**, *37*, 997–1008.
[39] $\beta_1=[M(NH_3)^{2+}]\times[NH_3]^{-1}\times[M^{2+}]^{-1}$, the values refer to 25 °C, $\mu=1$ M and are from reference [37].
[40] K. Hegetschweiler, R. D. Hancock, M. Ghisletta, T. Kradolfer, V. Gramlich, H. W. Schmalle, *Inorg. Chem.* **1993**, *32*, 5273–5284.
[41] T. Gajda, Y. Düpre, I. Török, J. Harmer, A. Schweiger, J. Sander, D. Kuppert, K. Hegetschweiler, *Inorg. Chem.* **2001**, *40*, 4918–4927.
[42] J. J. Perry, J. A. Perman, M. J. Zaworotko, *Chem. Soc. Rev.* **2009**, *38*, 1400–1417.
[43] In this paper, the term pH* refers to the direct pH-meter reading (Metrohm 713 pH meter) for D_2O samples using a Metrohm glass electrode with an aqueous (H_2O) Ag/AgCl-reference that was calibrated with aqueous (H_2O) buffer solutions. For the interconversion of pH* and pD see: L. Alderighi, A. Bianchi, L. Biondi, L. Calabi, M. De Miranda, P. Gans, S. Ghelli, P. Losi, L. Paleari, A. Sabatini, A. Vacca, *J. Chem. Soc. Perkin Trans. 2* **1999**, 2741–2745.
[44] HyperChem, Release 7.51 for Windows, Hypercube Inc., Gainsville, **2002**.
[45] a) MOMEC97, a molecular modeling package for inorganic compounds, P. Comba, T. W. Hambley, G. Lauer, N. Okon, University of Heidelberg, **1997**; b) J. E. Bol, C. Buning, P. Comba, J. Reedijk, M. Ströhle, *J. Comput. Chem.* **1998**, *19*, 512–523; c) P. Comba, T. W. Hambley, *Molecular Modeling of Inorganic Compounds*, VCH, Weinheim, **1995**.
[46] A. M. T. Bygott, A. M. Sargeson, *Inorg. Chem.* **1998**, *37*, 4795–4806.
[47] NMR-Tit, Program for the Simulation of pH Dependent Shifts in NMR Spectra, Version 2.0, A. Ries, K. Hegetschweiler, Saarbrücken, **1999**.
[48] S. Steinhauser, U. Heinz, M. Bartholomä, T. Weyhermüller, H. Nick, K. Hegetschweiler, *Eur. J. Inorg. Chem.* **2004**, 4177–4192.
[49] P. Gans, A. Sabatini, A. Vacca, *Talanta* **1996**, *43*, 1739–1753.
[50] a) Specfit/32 Version 3.0, Spectrum Software Associates, R. A. Binstead, B. Jung, A. D. Zuberbühler, Marlborough, **2000**; b) H. Gampp, M. Maeder, C. J. Meyer, A. D. Zuberbühler, *Talanta* **1985**, *32*, 95–101.
[51] B. Carlsson, G. Wettermark, *J. Inorg. Nucl. Chem.* **1976**, *38*, 1525–1527.
[52] G. M. Sheldrick, *Acta Crystallogr. Sect. A* **2008**, *64*, 112–122.
[53] Program used: PowderCell for Windows, Version 2.4, W. Kraus, G. Nolze, Federal Institute for Materials Research and Testing, Berlin, **2000**.

Received: September 16, 2009
Published online: February 8, 2010

